Inorganic Chemistry

Article

pubs.acs.org/IC

Electrochemical Behavior of Phosphine-Substituted Ruthenium(II) Polypyridine Complexes with a Single Labile Ligand

Go Nakamura,[†,‡] Masaya Okamura,[†,‡] Masaki Yoshida,[‡,$] Takayoshi Suzuki,[§] Hideo D. Takagi,[∥] Mio Kondo,[†,‡,⊥,#] and Shigeyuki Masaoka*[,†,‡,⊥]

[†]Department of Structural Molecular Science, School of Physical Sciences, The Graduate University for Advanced Studies (SOKENDAI), Shonan Village, Hayama-cho, Kanagawa 240-0193, Japan

[‡]Institute for Molecular Science (IMS), 5-1 Higashiyama, Myodaiji, Okazaki, Aichi 444-8787, Japan

[§]Graduate School of Natural Science and Technology, Okayama University, 3-1-1 Tsushima-naka, Kita-ku, Okayama 700-8530, Japan

[∥]Graduate School of Science and Research Center for Material Science, Nagoya University, Furo-cho, Chikusa-ku, Nagoya, Aichi 464-8602, Japan

[⊥]Research Center of Integrative Molecular Systems (CIMoS), 38 Nishigo-naka, Myodaiji, Okazaki, Aichi 444-8585, Japan

[#]Japan Science and Technology Agency (JST), ACT-C, 4-1-8 Honcho, Kawaguchi, Saitama 332-0012, Japan

Supporting Information

ABSTRACT: A series of phosphine-substituted ruthenium polypyridine complexes, *cis(P,Cl)*-[Ru(trpy)(Pqn)Cl]PF_6 (***cis*-Cl**), *trans(P,MeCN)*-[Ru(trpy)(Pqn)(MeCN)]$(PF_6)_2$ (***trans*-PN**), *cis(P,MeCN)*-[Ru(trpy)(Pqn)(MeCN)]$(PF_6)_2$ (***cis*-PN**), and [Ru(trpy)(dppbz)(MeCN)]$(PF_6)_2$ (**PP**), were synthesized and crystallographically characterized (trpy = 2,2′:6′,2″-terpyridine, Pqn = 8-(diphenylphosphanyl)quinoline, and dppbz = 1,2-bis(diphenylphosphanyl)benzene). In electrochemical measurements for ***cis*-PN** and **PP**, the reduction of ***cis*-PN** resulted in the formation of ***trans*-PN** via *cis*−*trans* isomerization and that of **PP** proceeded via a two-electron-transfer reaction. The mechanism of the electrochemical behaviors is discussed through consideration of five-coordinated species, $[Ru(trpy)(Pqn)]^{n+}$ or $[Ru(trpy)(dppbz)]^{n+}$ (n = 0−2), formed by liberation of a monodentate labile ligand.

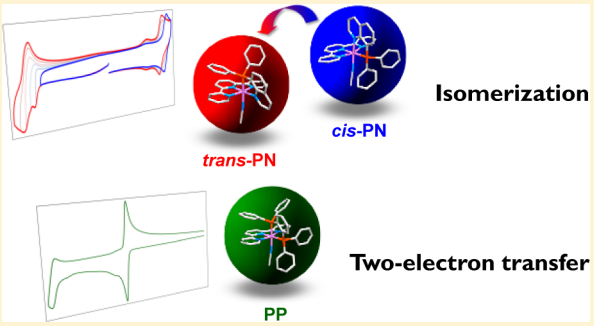

INTRODUCTION

Ruthenium(II) polypyridine complexes have been studied to gain knowledge of fundamental coordination chemistry, electrochemistry, photochemistry, and photophysics[1,2] and also to find potential applications to energy conversion, luminescent sensors, electroluminescence displays, and biotechnology.[3−6] Of particular interest are ruthenium(II) complexes containing tridentate and bidentate polypyridine ligands and a monodentate labile ligand, $[Ru(N{-}N{-}N)(N{-}N)(L)]^{n+}$ (N−N−N = tridentate polypyridine ligand, N−N = bidentate polypyridine ligand, and L = monodentate labile ligand), because these complexes can act as catalysts for chemical conversions such as oxidation,[7−10] reduction,[11−13] and photoinduced reactions.[14]

Ruthenium(II) phosphine complexes are also attractive targets for potential applications to photophysics[15] and catalysis[16−19] because the introduction of phosphine ligands can control electronic structures of the ruthenium center due to σ-donating and π-accepting abilities. Thus, the introduction of phosphine ligands to ruthenium(II) polypyridine complexes should be one of the key strategies in developing metal complexes with novel properties and reactivities. In fact, there have been several examples of ruthenium(II) polypyridine complexes containing monodentate phosphine ligands.[20,21] However, surprisingly, few studies examining substitution of phosphine for pyridine moiety in $[Ru(N{-}N{-}N)(N{-}N)(L)]^{n+}$-type complexes have been reported; there have been only a few studies of diphosphine-coordinated ruthenium(II) polypyridine complexes, $[Ru(N{-}N{-}N)(P{-}P)(L)]^{2+}$ (P−P = diphosphine ligand), and no crystal structures have been reported.[22] In addition, no studies involving the introduction of only one phosphine moiety into $[Ru(N{-}N{-}N)(N{-}N)(L)]^{n+}$-type complexes, e.g., $[Ru(P{-}N{-}N)(N{-}N)(L)]^{2+}$ or $[Ru(N{-}N{-}N)(P{-}N)(L)]^{2+}$, have been reported. Thus, the investigation of phosphine-substituted $[Ru(N{-}N{-}N)(N{-}N)(L)]^{n+}$-type complexes is important not only for the design and development of new catalysts but also for an understanding of their basic properties.

This report describes the syntheses, structural characterization, and electrochemical and spectroscopic properties of a series of ruthenium(II) polypyridine complexes containing 8-

Received: February 14, 2014
Published: June 25, 2014

   dx.doi.org/10.1021/ic5003644 | *Inorg. Chem.* 2014, 53, 7214−7226

(diphenylphosphanyl)quinoline (Pqn), *cis(P,Cl)*-[Ru(trpy)(Pqn)Cl]PF_6 (***cis*-Cl**) and *trans(P,MeCN)*- and *cis(P,MeCN)*-[Ru(trpy)(Pqn)(MeCN)]$(PF_6)_2$ (***trans*-PN** and ***cis*-PN**, trpy = 2,2′:6′,2″-terpyridine), or 1,2-bis(diphenylphosphanyl)benzene (dppbz), [Ru(trpy)(dppbz)(MeCN)]$(PF_6)_2$ (**PP**) (Scheme 1).

Scheme 1. Structures of a Tridentate Ligand (trpy) and Bidentate Ligands (bpy, Pqn, and dppbz) Used in This Study

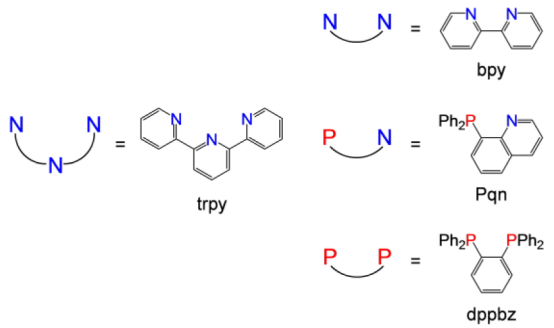

Effects of the number and position of phosphine donors on the structures and electronic properties also were investigated on the basis of comparisons with [Ru(trpy)(bpy)(MeCN)]$(PF_6)_2$ (**NN**).[9,12,13,23,24] Control over the spectroscopic and electrochemical properties is expected to be achieved by changing the number and position of phosphine donors in [Ru(N−N−N)(N−N)(L)]$^{n+}$-type complexes. Indeed, characteristics of crystal structures and spectroscopic properties were simply explained through σ donation and π back-donation of phosphine donors. However, the electrochemical measurements of these complexes showed distinct behavior in their reduction reactions; reduction of ***cis*-PN** resulted in *cis*−*trans* isomerization to ***trans*-PN**, and that of **PP** proceeded via a two-electron-transfer reaction (Scheme 2). The mechanism of these electrochemical behaviors was explained in conjunction with the liberation of a monodentate labile ligand.

RESULTS

Synthesis. ***trans*-PN**, ***cis*-PN**, and **PP** were synthesized according to the reactions shown in Scheme 3, while **NN** was prepared by a method reported previously.[25] The unsymmetrical bidentate Pqn ligand, which contains diphenylphosphanyl and quinolyl groups, was used for the syntheses of the two geometrical isomers ***trans*-PN** and ***cis*-PN** and can form a strain-free five-membered chelate ring similarly to 2,2′-bipyridine (bpy) or 1,10-phenanthroline (phen).[26]

cis*-Cl**, the PF_6^- salt of the chloro precursor for ***trans*-PN** and ***cis*-PN**, was synthesized by the reaction of [Ru(trpy)Cl_3]·H_2O[27] with Pqn, followed by the addition of an aqueous solution of $NaPF_6$. The $^{31}P\{^1H\}$ NMR spectrum of ***cis*-Cl** in CD_3CN showed a singlet at δ 51.16. ^1H and $^{31}P\{^1H\}$ NMR spectroscopy confirmed that isomerization and ligand substitution of ***cis*-Cl** does not occur in acetonitrile at room temperature. The preparation of single crystals of ***cis*-Cl** suitable for X-ray crystallography was not successful. Crystals suitable for the analysis were obtained as the BPh_4^- salt, *cis(P,Cl)*-[Ru(trpy)(Pqn)Cl]BPh_4 (cis*-Cl′**), prepared by an ion-exchange reaction from PF_6^- to BPh_4^-. Note that the *trans* complex was isolated not as the Cl-coordinated form but as the solvent-coordinated form in the reaction of [Ru(trpy)Cl_3]·H_2O with Pqn. Although an unidentified compound was detected in the ^1H NMR spectrum of the reaction mixture (Figure S2, Supporting Information), further treatment of the mixture with acetonitrile afforded the MeCN-coordinated complex ***trans*-PN** as a byproduct of the reaction; ***trans*-PN** was identified by ^1H and $^{31}P\{^1H\}$ NMR spectra. This may be due to easy dissociation of the chloride ligand at the *trans* position of the phosphino group in *trans(P,Cl)*-[Ru(trpy)(Pqn)Cl]$^+$ (***trans*-Cl**), which affords *trans(P,L)*-[Ru(trpy)(Pqn)(L)]$^{2+}$ (L = monodentate labile ligand; e.g., solvent molecules) through the *trans*-labilizing effect.[28]

Scheme 2. Schematic Illustration of Electrochemical Reduction Reactions for (a) *trans*-PN, (b) *cis*-PN, and (c) PP[a]

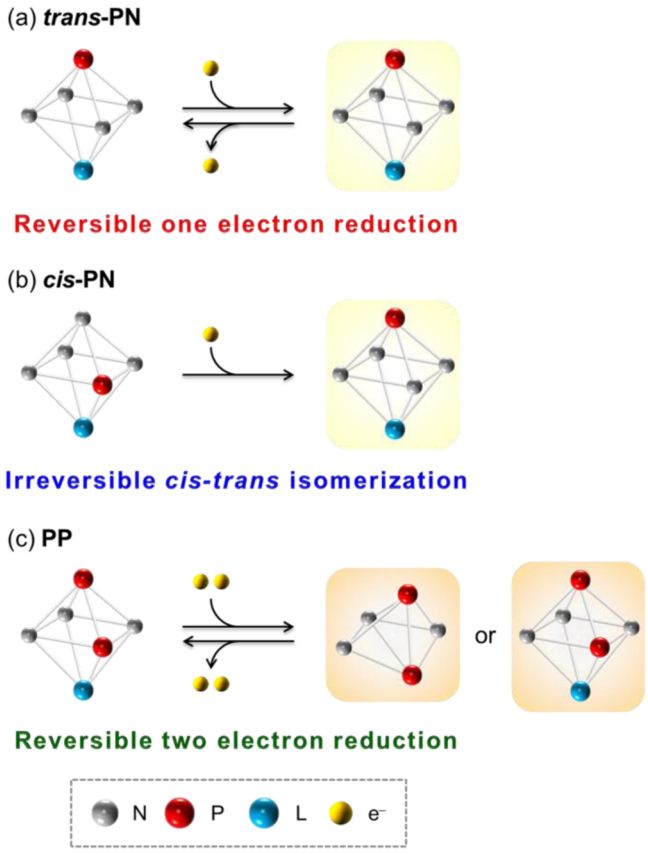

[a]Each polyhedron represents a ruthenium polypyridine complex with a phosphine donor (P) and a monodentate labile ligand (L).

Reaction of ***cis*-Cl** with an equimolar amount of $AgPF_6$ in a 2/1 mixture of 2-butanone and water at 100 °C and further treatment with MeCN gave ***trans*-PN** as a major product, and the product was characterized by ^1H NMR spectroscopy. The *cis* isomers were not detected under these reaction conditions. The $^{31}P\{^1H\}$ NMR spectrum of ***trans*-PN** in CD_3CN showed a singlet at δ 58.80, similar to the signal reported for [Ru(bpy)$_2$(Pqn)]$(PF_6)_2$ (δ 58.81 (s)).[29] Note that a solvent with a high boiling point is required to obtain ***trans*-PN** because the isomerization of ***cis*-Cl** or the formed ***cis*-PN** to the corresponding *trans* complex during the reaction is required. (For details of heat-induced isomerization behavior, see Solvent-Induced and Photoinduced Isomerization.)

In contrast, the reaction of ***cis*-Cl** with an equimolar amount of $AgPF_6$ in acetonitrile at 70 °C gave ***cis*-PN** as a major product, which was confirmed by ^1H NMR spectroscopy. Recrystallization from diethyl ether/chloroform/acetonitrile yielded ***cis*-PN** as orange crystals. The $^{31}P\{^1H\}$ NMR spectrum

dx.doi.org/10.1021/ic5003644 | Inorg. Chem. 2014, 53, 7214−7226

Scheme 3. Syntheses of *cis*-Cl, *trans*-PN, *cis*-PN, and PP

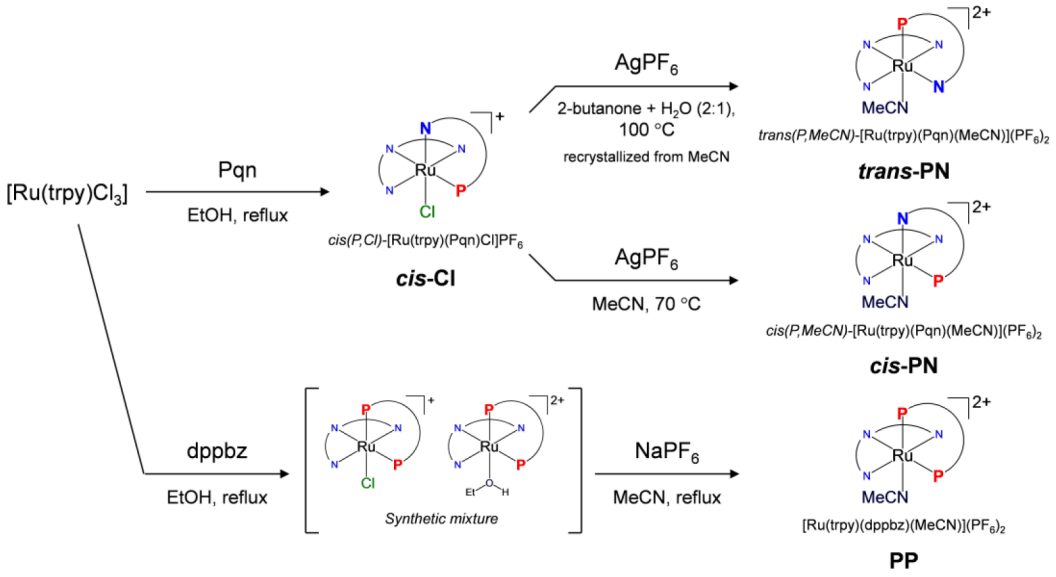

of ***cis*-PN** in CD_3CN gave a singlet at δ 55.96, showing an upfield shift ($\Delta\delta$ = 2.84) in comparison to the signal in the spectrum of ***trans*-PN**.

It should be noted that there have been several reports on photolabile ruthenium polypyridyl complexes.[10,30] Therefore, syntheses of ***cis*-Cl**, ***trans*-PN**, and ***cis*-PN** were also performed in the dark. However, the effect of light shielding on the yields of products is negligible (Table S3, Supporting Information), suggesting that photoisomerization of these complexes does not proceed under the synthetic conditions.

The ruthenium diphosphine complex **PP** was produced by the reaction of $[Ru(trpy)Cl_3]\cdot H_2O$ with 1 equiv of dppbz. The reaction in ethanol afforded a mixture of $[Ru(trpy)(dppbz)Cl]^+$ and $[Ru(trpy)(dppbz)(EtOH)]^{2+}$. The resulting mixture was then refluxed in acetonitrile to afford **PP**. The $^{31}P\{^1H\}$ NMR spectrum of **PP** in CD_3CN afforded two doublets at δ 68.57 and 69.77 with coupling constants of 20.2 Hz. These peak positions are similar to those of $[Ru(bpy)_2(dppbz)](PF_6)_2$ (δ 69.51 (s)).[29]

Crystal Structures. The molecular structures of ***cis*-Cl′**, ***cis*-PN**, ***trans*-PN**, and **PP** were determined by single-crystal X-ray crystallography. The crystallographic data are shown in Table S1 in the Supporting Information. ***cis*-Cl′** crystallizes with two crystallographically independent ruthenium complexes, two BPh_4 anions, and one acetonitrile molecule as the crystal solvent in the asymmetric unit of the triclinic $P\bar{1}$ space group. No significant difference exists between the structures of the two independent ruthenium complexes. An ORTEP drawing of one of the cationic moieties of ***cis*-Cl′** is shown in Figure 1. Two chelate ligands, trpy and Pqn, coordinate to the metal ion in a perpendicular manner to form a distorted-octahedral geometry at the ruthenium atom, where the phosphorus donor of Pqn and the chloro ligand are located in *cis* positions of the octahedron. Bond distances between the ruthenium atom and middle nitrogen atom of trpy (Ru1−N2 and Ru2−N6) of ***cis*-Cl′** are 2.018(3) and 2.011(4) Å, respectively, and are significantly longer than that of the 2,2′-bipyridine analogue (1.951(2) Å for $[Ru(trpy)(bpy)Cl]PF_6$). In contrast, the Ru−Cl distances (2.4049(11) and 2.4102(12) Å for Ru1−Cl1 and Ru2−Cl2, respectively) are similar to that of $[Ru(trpy)(bpy)Cl]PF_6$ (2.3969(7) Å).[31]

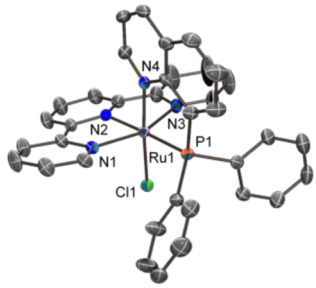

Figure 1. ORTEP drawing (50% probability level) of one of the cationic complexes in ***cis*-Cl′**. Hydrogen atoms are omitted for clarity.

The asymmetric unit of the monoclinic $P2_1/c$ crystal of ***trans*-PN** contained one cationic ruthenium complex, two PF_6 anions, and one dichloromethane molecule. An ORTEP drawing of the cationic moiety is shown in Figure 2a, and selected bond distances and angles are presented in Figure 3 and Table S2 (Supporting Information). Trpy and Pqn coordinate to the ruthenium center in a mutually perpendicular manner and create a distorted-octahedral environment, where the phosphorus donor of Pqn and nitrogen atom of the acetonitrile ligand are located in *trans* positions. The bond distance between the ruthenium atom and nitrogen atom of the acetonitrile ligand is 2.127(5) Å, which is longer than that found in **NN** (2.03(1) Å)[24] due to the stronger trans influence of the phosphorus atom of Pqn in comparison to that of the nitrogen atom of bpy.

The crystals of ***cis*-PN** showed a triclinic $P\bar{1}$ space group with one cationic ruthenium complex, two PF_6 anions, and one chloroform molecule as the asymmetric unit. The structure of the cationic moiety of ***cis*-PN** (Figure 2b) was basically similar to that of ***cis*-Cl′**, except for coordination of an acetonitrile ligand instead of an anionic chloro ligand. The bond distance between the ruthenium atom and nitrogen atom of the acetonitrile ligand is 2.041(2) Å, which is much shorter than that of ***trans*-PN** (2.127(5) Å) but is similar to that of **NN** (2.03(1) Å). The bond distance between the ruthenium atom and the middle nitrogen atom of trpy (Ru1−N2, 2.033(2) Å) in ***cis*-PN** is significantly longer than those of ***trans*-PN** (1.967(5) Å) and **NN** (1.953(8) Å), due to the *trans* influence

dx.doi.org/10.1021/ic5003644 | Inorg. Chem. 2014, 53, 7214−7226

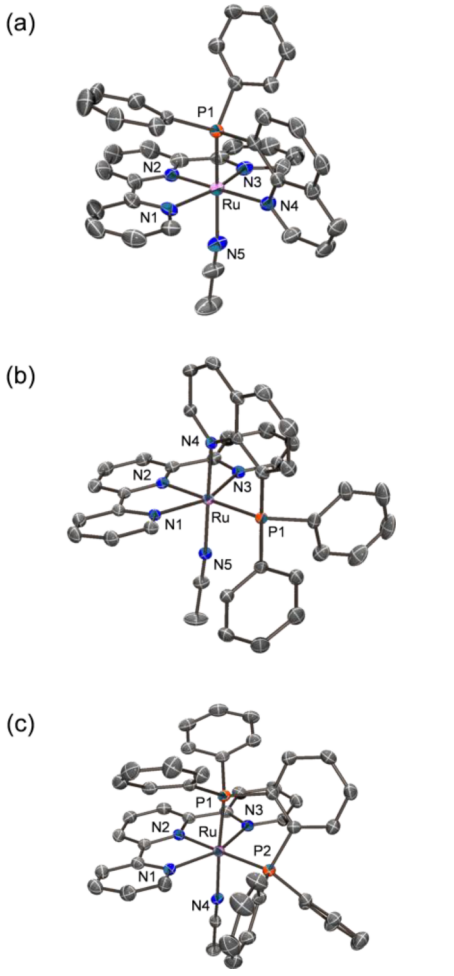

Figure 2. ORTEP drawings (50% probability level) of the cationic complexes in (a) ***trans*-PN**, (b) ***cis*-PN**, and (c) **PP**. Hydrogen atoms are omitted for clarity.

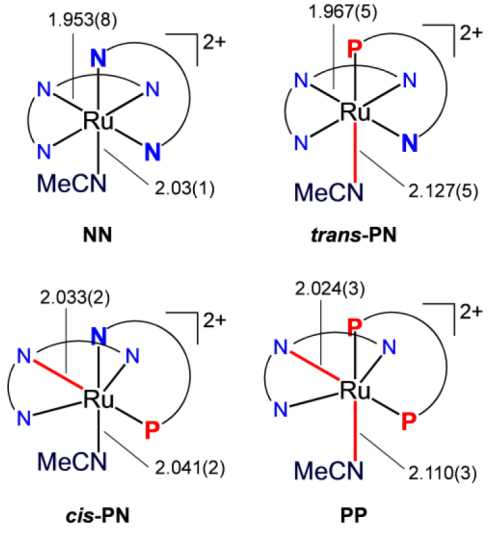

Figure 3. Comparison of bond distances (Å) around ruthenium centers of **NN**, ***trans*-PN**, ***cis*-PN**, and **PP**.

of the phosphorus atom of Pqn. For the same reason, the average value of the N–Ru–N bite angles of the [Ru(trpy)] moiety in ***cis*-PN** (77.9°) is much smaller than those in ***trans*-PN** (79.5°) and **NN** (79.9°).

PP crystallizes with one ruthenium complex, two PF_6 anions, and one dichloromethane molecule as the asymmetric unit in the orthorhombic *Pbca* space group. An ORTEP drawing of the cationic moiety is shown in Figure 2c, and selected bond distances and angles are shown in Table S2 (Supporting Information). The Ru–N(MeCN) bond distance of in **PP** is 2.110(3) Å, which is much longer than those in ***cis*-PN** and **NN** and is close to that in ***trans*-PN**. The long Ru–N distance (Ru1–N2, 2.024(3) Å) and small N–Ru–N bite angles (average 78.0°) of the [Ru(trpy)] moiety in **PP** are also affected significantly by the *trans* influence of the phosphorus atom of dppbz.

UV–Vis Absorption Spectra. Figure 4 shows the UV–vis absorption spectra of the series $[Ru(trpy)(BL)(MeCN)](PF_6)_2$

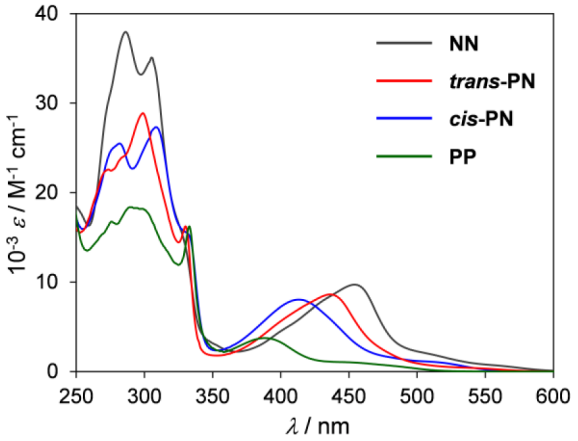

Figure 4. UV–vis absorption spectra of **NN**, ***trans*-PN**, ***cis*-PN**, and **PP** in acetonitrile at room temperature.

(**NN**, ***trans*-PN**, ***cis*-PN**, and **PP**), where BL is a bidentate ligand such as bpy, Pqn, or dppbz. Spectral data for these four complexes and related compounds[29] are given in Table 1. All of the complexes display intense absorption bands in the UV region, assigned to ligand-based $\pi-\pi^*$ transitions. Additionally, a moderately intense band in the visible region for each complex is assigned to the metal-to-ligand charge transfer (MLCT) transition from the dπ orbitals of ruthenium to the π^* orbitals of trpy and BL. The absorption maxima (λ_{max}) of the MLCT transitions of ***trans*-PN**, ***cis*-PN**, and **PP** were blue-shifted in comparison with that of **NN**. The degrees of the blue shifts ($\Delta\lambda_{complex}(MLCT) = \lambda_{max,NN}(MLCT) - \lambda_{max,complex}(MLCT)$) were 18 nm for ***trans*-PN**, 41 nm for ***cis*-PN**, and 66 nm for **PP**. A similar blue shift of the MLCT band was also observed in the series $[Ru(bpy)_2(BL)]^{2+}$ (Table 1),[29] which is attributed to the stabilization of the dπ orbitals of the ruthenium center upon introduction of the phosphine donors. Note that the MLCT transition energy of ***cis*-PN** experienced a larger shift than that of ***trans*-PN** despite the isomeric relationship between ***trans*-PN** and ***cis*-PN**, suggesting that the position of the phosphorus atom affects the electronic structure of the complexes (for a detailed explanation of phosphorus atom affects, please see Phosphine as σ-Donor and π-Acceptor in the Discussion). The molar absorption coefficient of **PP** was nearly half those of **NN**, ***trans*-PN**, and ***cis*-PN**.

Electrochemistry. The cyclic voltammograms (CVs) of **NN**, ***trans*-PN**, ***cis*-PN**, and **PP** are shown in Figure 5. Electrochemical data of these complexes and related com-

dx.doi.org/10.1021/ic5003644 | Inorg. Chem. 2014, 53, 7214–7226

Table 1. UV−Vis Absorption Data (λ_{max}/nm (10^{-3} ϵ/M^{-1} cm^{-1})) and Redox Potentials ($E_{1/2}$/V vs Fc/Fc^+) for NN, *trans*-PN, *cis*-PN, PP, and Related Compounds in Acetonitrile at Room Temperature

	λ_{max}		reduction			
complex	MLCT transition	$\pi-\pi^*$ transition	$E_{1/2}(1)$	$E_{1/2}(2)$	$E_{1/2}(3)$	oxidation $E_{1/2}(Ru^{II/III})$
NN[a]	454 (9.72)	325 (16.58),[d] 305 (27.24), 286 (37.95), 273 (29.83)[d]	−1.65	−1.95		+0.92
***trans*-PN**	436 (8.62)	330 (16.25), 299 (28.89), 284 (23.97)[d], 274 (22.57)	−1.70[e]	−1.77[e]	−2.13	+0.97
***cis*-PN**	413 (8.05)	332 (15.40)[d], 309 (27.31), 282 (25.48), 275 (24.57)	*f*	*f*	*f*	+1.05
PP	388 (3.76)	333 (16.24), 301 (18.01)[d], 290 (18.36), 276 (16.77)	−1.50[e]	−1.46[e]	−2.49	+1.27
$[Ru(bpy)_3](PF_6)_2$[b]	452 (13.2), 410 (7.48)[d]	287 (77.2)	−1.86	−2.02		+0.75
$[Ru(bpy)_2(Pqn)](PF_6)_2$[b]	418 (10.02)	285 (46.98)	−1.80	−2.03		+0.91
$[Ru(bpy)_2(dppbz)](PF_6)_2$[b]	377 (8.09)	319 (15.65),[d] 278 (34.92)	−1.82	−2.07		+1.18
$[Ru(trpy)_2](PF_6)_2$[c]	475 (14.7)	308 (63.4), 270 (38.8)	−1.66	−1.90		+0.89

[a]See also ref 23. [b]Reference 29. [c]Reference 31. [d]Absorption shoulder. [e]Simulated values. See also Table S4 (Supporting Information). These two redox couples of **PP** at −1.50 and −1.46 V were observed as a single wave with $E_{1/2}$ = −1.47 V. [f]***cis*-PN** underwent isomerization to ***trans*-PN** upon reduction.

pounds are given in Table 1. The CVs were measured in 0.1 M tetraethylammonium perchlorate (TEAP)/acetonitrile. All complexes displayed one reversible oxidation wave, which was assigned to a Ru(III)/Ru(II) redox couple. The half-wave potentials ($E_{1/2}$) of **NN**, ***trans*-PN**, ***cis*-PN**, and **PP** were +0.92, +0.97, +1.05, and +1.27 V vs ferrocene/ferrocenium (Fc/Fc^+), respectively. The positive shift on introduction of the phosphine donors is due to the stabilization of the dπ orbitals of the ruthenium center (for details, see Phosphine as σ-Donor and π-Acceptor in the Discussion). This tendency was also observed in the series $[Ru(bpy)_2(BL)]^{2+}$ (Table 1).[29] Note that the oxidation potential of ***cis*-PN** was more positive than that of ***trans*-PN**.

CVs in the negative potential region are shown in Figure 5b. Each complex exhibited distinct electrochemical behavior, unlike those in the positive potential region. The CV of ***trans*-PN** showed two redox waves at $E_{1/2}$ = −1.73 and −2.13 V. The results of controlled-potential electrolysis (CPE), square wave voltammetry (SWV), and the CV simulation of the wave at $E_{1/2}$ = −1.73 V indicate that two one-electron processes with similar redox potentials ($E^{\circ\prime}{}_1$(***trans*-PN**) = −1.70 V and $E^{\circ\prime}{}_2$(***trans*-PN**) = −1.77 V) exist in this region (Figure S5, Supporting Information). The first reduction potentials ($E_{1/2}(1)$) of **NN** (−1.65 V) and ***trans*-PN** (−1.70 V) are assigned to reduction of the trpy ligand.[32]

The CV of ***cis*-PN** at a scan rate of 100 mV/s showed an irreversible reduction peak at E_{pc} = −1.56 V, followed by two reversible redox waves at $E_{1/2}$ = −1.73 and −2.13 V. The two reversible redox waves of ***cis*-PN** are very similar to those of ***trans*-PN** (Figure S6a), which implies that irreversible and rapid isomerization of ***cis*-PN** to ***trans*-PN** occurred on the electrode surface along with reduction of ***cis*-PN** (for a detailed mechanism of the electrochemically induced isomerization behavior of the complex, see Mechanism of Isomerization and Electrochemical Behavior).

To further investigate the *cis*−*trans* transformation, potentials were swept in a positive or negative direction from the open circuit potential (−0.19 V) at a scan rate of 1.0 V/s in a ***cis*-PN** solution (Figure S6b, Supporting Information). The positive-direction sweeping showed an oxidation wave at $E_{1/2}$ = 1.05 V, which is assigned to a Ru(III)/Ru(II) redox couple of ***cis*-PN**. In contrast, the negative-direction sweeping showed that the $E_{1/2}$ value matched that of ***trans*-PN** ($E_{1/2}$ = 0.97 V). Figure 6 shows CVs of ***cis*-PN** at a scan rate of 1.0 V/s, for which the negative edges of potential sweeping were changed between −1.5 and −2.0 V at an interval of 0.1 V. The results clearly indicate that ***cis*-PN** is converted to ***trans*-PN** upon the electrochemical reduction reaction and that the *cis*−*trans* conversion occurs after the first irreversible reduction around −1.6 V. The first irreversible reduction peak of ***cis*-PN** (−1.6 V) is probably due to electron insertion into the π^* orbital of the trpy ligand. The electrochemical behavior of ***cis*-PN** and ***trans*-PN** is summarized in Scheme 4.

For **PP**, the first reduction wave was observed at $E_{1/2}$ = −1.47 V with a peak potential separation ΔE_p of 41 mV (where $\Delta E_p = E_{pa} - E_{pc}$). The $E_{1/2}$ value was relatively positive in comparison to those of the analogues **NN** (−1.65 V), ***trans*-PN** (−1.70 V), and $[Ru(bpy)_2(dppbz)](PF_6)_2$ (−1.82 V).[29] The number of electrons transferred in the first reduction wave of **PP** was determined to be 2.13 by CPE (Figure S3, Supporting Information). The results of CV simulation gave the two redox potentials $E^{\circ\prime}{}_1$(**PP**) = −1.50 V and $E^{\circ\prime}{}_2$(**PP**) = −1.46 V vs Fc/Fc^+, indicating the potential inversion of two redox processes (Figure S5, Supporting Information). These results indicate that the first reduction step of **PP** is a two-electron-transfer process with potential inversion. Subsequent reduction was observed in a much lower negative potential region (−2.49 V).

DFT Calculations. To discuss the electronic structures of ***trans*-PN**, ***cis*-PN**, and **PP**, density functional theory (DFT) calculations were conducted using the Gaussian 09 programs[33] with the B3LYP functional[34,35] and LanL2DZ basis set.[36] All calculations were performed with the polarizable continuum model (PCM)[37] to account for solvent effects in acetonitrile.

The highest occupied molecular orbitals (HOMOs, HOMO to HOMO−2) and the lowest unoccupied molecular orbitals (LUMOs, LUMO to LUMO+2) are illustrated in Figure S8 (Supporting Information). The HOMOs of ***trans*-PN** and ***cis*-PN** contain dπ (d_{xy}, d_{yz}, and d_{zx}) characteristics of ruthenium with distribution to the π^* orbitals of trpy, Pqn, and acetonitrile ligands and σ^* orbitals of P−C bonds in the phosphine donors. The LUMOs are dominated mainly by π^* orbitals of trpy or Pqn. The frontier orbitals of **PP** are similar to those of ***trans*-PN** and ***cis*-PN**, except that the π^* orbitals of dppbz are not

dx.doi.org/10.1021/ic5003644 | Inorg. Chem. 2014, 53, 7214−7226

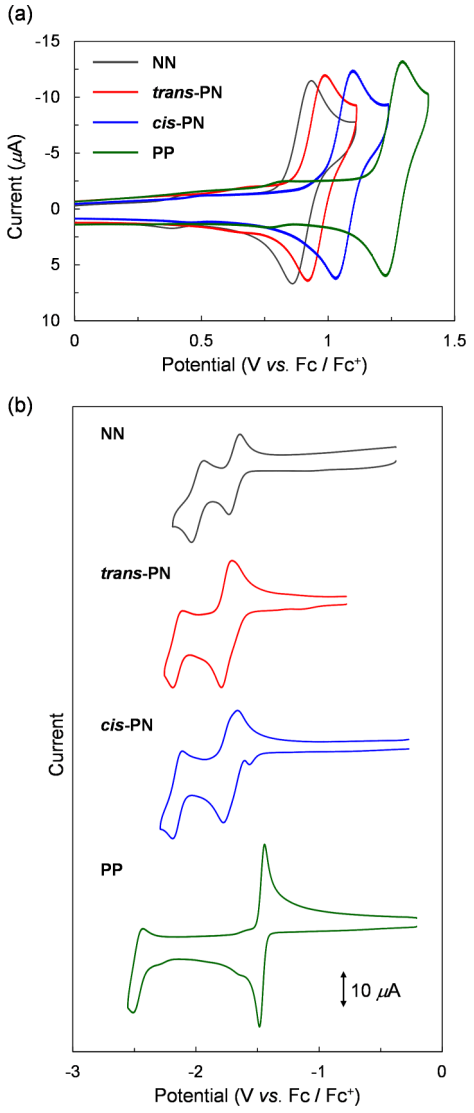

Figure 5. Cyclic voltammograms of **NN**, ***trans*-PN**, ***cis*-PN**, and **PP** (0.5 mM) in 0.1 M TEAP/acetonitrile under an Ar atmosphere scanned in the (a) positive and (b) negative regions (working electrode, glassy carbon; counter electrode, Pt wire; reference electrode, Ag/Ag^+; scan rate, 100 mV/s).

involved in orbitals from HOMO−2 to LUMO+2. The HOMO energy levels of ***trans*-PN**, ***cis*-PN**, and **PP** were −6.24, −6.30, and −6.53 eV (Figure S9, Supporting Information), respectively, indicating a tendency similar to that observed in the oxidation potentials in cyclic voltammograms (+0.97, +1.05, and +1.27 V vs Fc/Fc^+, see Table 1), as discussed above.

Electronic transitions for the complexes were investigated using the time-dependent density functional theory (TD-DFT) method.[38] Calculated excitation wavelengths and oscillator strengths for selected transitions are given in Table S5 (Supporting Information), and absorption spectra based on these calculated transitions with Gaussian functions are depicted in Figure 7. The profiles of convoluted absorption spectra are similar to those observed experimentally. For ***trans*-PN** and ***cis*-PN**, transitions in the visible light region arise mainly from the MLCT transition from the $d\pi$ orbitals of ruthenium (HOMOs) to the π^* orbitals of trpy (LUMO and LUMO+1) and Pqn (LUMO+2). For **PP**, the transitions arise

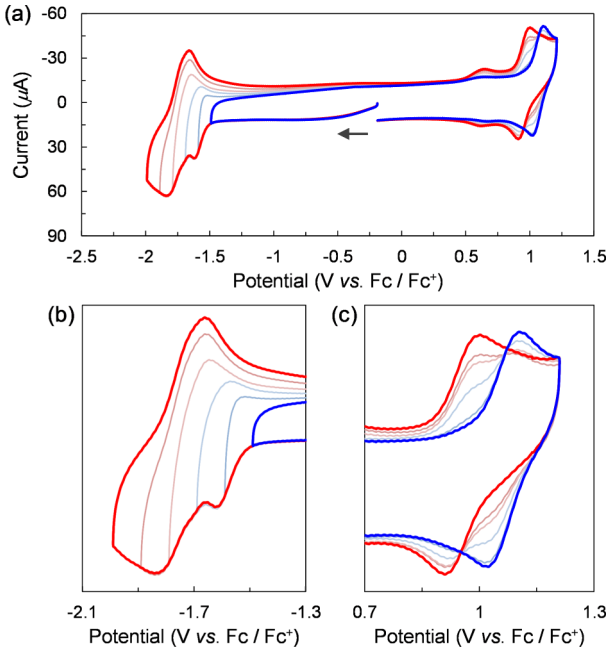

Figure 6. Cyclic voltammograms of ***cis*-PN** (0.5 mM) in 0.1 M TEAP/acetonitrile under an Ar atmosphere (working electrode, glassy carbon; counter electrode, Pt wire; reference electrode, Ag/Ag^+; scan rate, 100 mV/s): (a) full-scale view; (b) magnified view in the range −2.1 to −1.3 V; (c) magnified view in the range +0.7 to +1.3 V. Negative edges of potential sweeping were switched between −1.5 V (blue) and −2.0 V (red) at an interval of 0.1 V. Potential sweeps were started from the open circuit potential (−0.19 V).

Scheme 4. Electrochemical Behavior of *trans*-PN and *cis*-PN

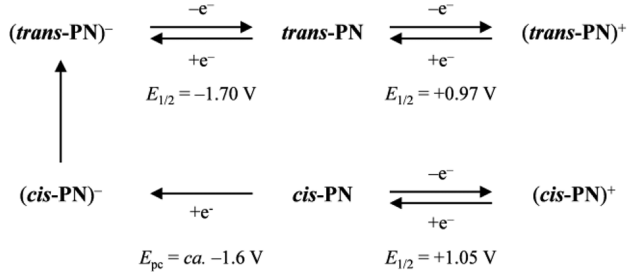

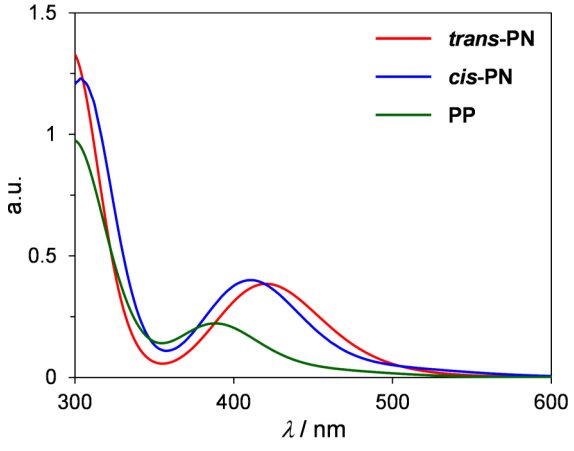

Figure 7. Simulated absorption spectra of ***trans*-PN**, ***cis*-PN**, and **PP** in acetonitrile on the basis of TD-DFT calculations.

dx.doi.org/10.1021/ic5003644 | Inorg. Chem. 2014, 53, 7214−7226

mainly from dπ orbitals of ruthenium (HOMOs) to π* orbitals of trpy (LUMO and LUMO+1), which do not involve the π* orbitals of dppbz. The intensity of the simulated absorption of **PP** was nearly 50% of those of ***trans*-PN** and ***cis*-PN**, which is consistent with the experimental results (Figure 4).

Solvent-Induced and Photoinduced Isomerization. Isomerization of ***cis*-PN** to ***trans*-PN** does not occur in acetonitrile, even upon heating to temperatures near the boiling point (75 °C) for 1 day (Figure S10, Supporting Information). In contrast, the isomerization proceeded upon moderate heating in *N*,*N*-dimethylformamide (DMF) or by visible-light irradiation (λ >370 nm).

The time course of spectral changes of ***cis*-PN** in DMF heated at 110 °C is shown in Figure 8. Note that the

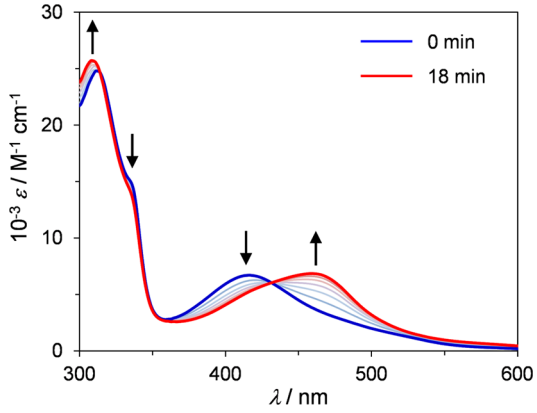

Figure 8. Time course of spectral changes of ***cis*-PN** in DMF at 110 °C. Spectra were recorded at 3 min intervals.

dissociation of the acetonitrile ligand was not observed for ***cis*-PN** in DMF (Figures S11 and S12, Supporting Information) at room temperature and the spectrum at 0 min was consistent with that of ***cis*-PN** at room temperature. The anchored isosbestic points at λ 314 and 432 nm indicate that only two species were involved without the formation of side products or intermediates. On the basis of comparisons with the absorption spectrum of ***trans*-PN** in DMF (Figure S11), the product of this isomerization reaction was identified as the DMF-coordinated *trans* isomer *trans(P,DMF)*-[Ru(trpy)(Pqn)(DMF)](PF$_6$)$_2$ (***trans*-PN^{DMF}**, λ_{max} for MLCT transition 462 nm). Therefore, the spectral change observed at 110 °C is attributed to the transformation from ***cis*-PN** to ***trans*-PN^{DMF}**.

The reaction kinetics of the transformation was investigated using UV−vis spectroscopy in DMF at 70, 80, 90, 100, and 110 °C. The spectral changes were analyzed using the singular value decomposition (SVD) method. The SVD-based spectral analysis in SPECFIT[39] confirms that the isomerization is first order at 70−110 °C with rate constants of k = [2.10(11)] × 10^{-5}, [7.5(4)] × 10^{-5}, [2.36(15)] × 10^{-4}, [6.05(14)] × 10^{-4}, and [1.52(5)] × 10^{-3} s^{-1}, respectively. The thermodynamic parameters for the conversion of ***cis*-PN** to ***trans*-PN^{DMF}** were calculated using the Eyring equation.[40] The Eyring plot shown in Figure 9 affords an entropy of activation ($\Delta S^{\ddagger}$) of 111(8) J mol^{-1} K^{-1} and an enthalpy of activation ($\Delta H^{\ddagger}$) of 120(3) kJ mol^{-1}. The large positive value of $\Delta S^{\ddagger}$ indicates the dissociative mechanism of this transformation.[40] The $\Delta H^{\ddagger}$ value (120(3) kJ mol^{-1}) appears to correspond to the dissociative energy of the Ru−N(MeCN) bond.[41] Therefore, the dissociation of an acetonitrile ligand is the isomerization rate determining step,

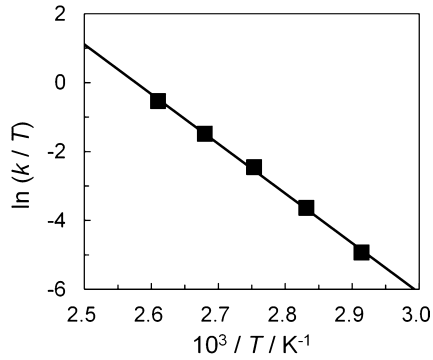

Figure 9. Eyring plot for the transformation of ***cis*-PN** to ***trans*-PN^{DMF}**.

followed by the coordination of a DMF molecule to give ***trans*-PN^{DMF}**. The half-life for the transformation from ***cis*-PN** to ***trans*-PN^{DMF}** in DMF is estimated to be longer than 1 year at room temperature (τ = 394 days at 20 °C), consistent with the fact that the acetonitrile ligand of ***cis*-PN** barely dissociates in DMF at room temperature.

Photo responses of obtained complexes were investigated by irradiating acetonitrile solutions of complexes with visible light. Under these experimental conditions, ***cis*-Cl** and ***trans*-PN** did not show a photo response (for details, see Figure S13 in the Supporting Information). In contrast, irradiation of an acetonitrile solution of ***cis*-PN** with visible light resulted in isomerization to ***trans*-PN**, which was monitored by UV−vis spectroscopy, as shown in Figure 10. The existence of isosbestic

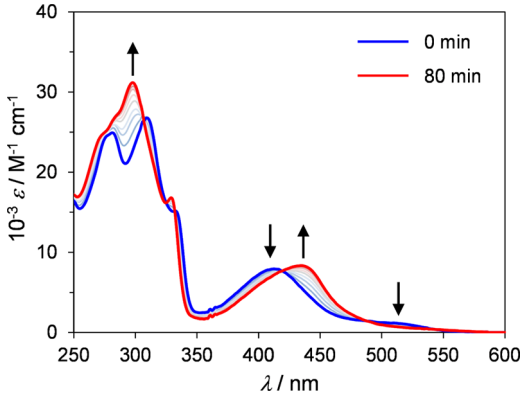

Figure 10. Time course of spectral changes of ***cis*-PN** under photoirradiation (λ >370 nm) in acetonitrile at room temperature. Spectra were recorded at 10 min intervals.

points at λ 307, 325, 332, 419, and 488 nm indicates that the isomerization proceeds without side products or stable intermediates. The kinetic profile of the photoisomerization process was first order with respect to the concentration of the complex. The rate constant was determined using the SVD method to be k = [4.2(6)] × 10^{-4} s^{-1} at room temperature. Along with the dissociative mechanism of solvent-induced isomerization in DMF, the photochemical isomerization is probably related to ligand dissociation from the triplet metal-centered (^{3}MC) state, which has antibonding nature between the metal ion and the acetonitrile ligand and is thermally accessible from the ^{3}MLCT photoexcited state.[10d]

Water Oxidation. As mentioned earlier, thee [Ru(N−N−N)(N−N)(L)]$^{n+}$-type ruthenium polypyridine complexes can serve as catalysts for some chemical conversions.[7−14] Because

dx.doi.org/10.1021/ic5003644 | Inorg. Chem. 2014, 53, 7214−7226

the reduction or photoirradiation can lead to *cis*−*trans* isomerization (see Electrochemistry), in the present study, water oxidation catalyses of ***trans*-PN** and ***cis*-PN**, together with that of **PP**, were investigated in order to examine the difference in reactivities between the geometrical isomers. The reaction was initiated by adding a solution of a catalyst in acetonitrile (0.1 mL) to a solution of $Ce(NH_4)_2(NO_3)_6$ (0.40 mmol) in water (1.9 mL) at 20 °C under an Ar atmosphere, where acetonitrile was used to improve the solubility of the PF_6^- salt of the catalyst. The oxygen evolved was monitored using an oxygen probe (YSI 5331/5300), and the results are shown in Figure 11. The turnover numbers (TON) of ***trans*-PN**, ***cis*-PN**, and **PP** after 1 h were determined to be 24.8, 6.7, and 0.4, respectively. The order of the catalytic activities is ***trans*-PN** > ***cis*-PN** > **PP**, although their activities are less than that of **NN**.[9] This order of catalytic activities matches the order of oxidation potentials of the ruthenium center shown in Table 1.

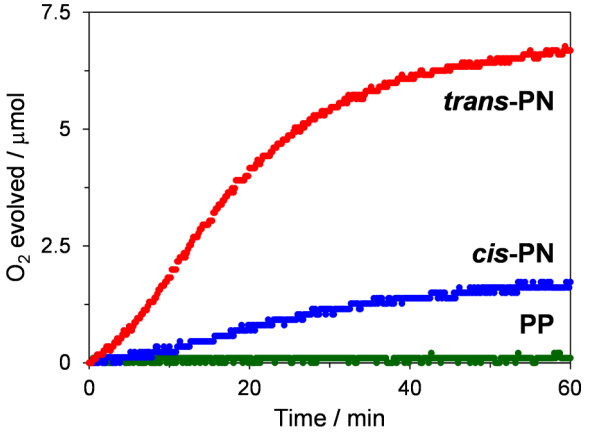

Figure 11. Oxygen evolution from a 19/1 water/acetonitrile mixture (2 mL) containing $Ce(NH_4)_2(NO_3)_6$ (200 mM) in the presence of ***trans*-PN**, ***cis*-PN**, or **PP** (0.125 mM) as a catalyst.

DISCUSSION

Phosphine as σ-Donor and π-Acceptor. The differences in the redox potentials and UV−vis absorption spectra among ***trans*-PN**, ***cis*-PN**, **PP**, and **NN** can be reasonably interpreted by considering the properties of the phosphine group.

The σ-donor character of the phosphine group significantly elongates the bond length between the ruthenium center and the ligand located at the position *trans* to the phosphine group, called the *trans* influence. The red lines in Figure 3 correspond to the elongated bonds. The σ donation also affects the kinetics of ligand substitution reactions. ***trans*-Cl**, the geometrical isomer of ***cis*-Cl**, was not isolated because the chloride ligand at the position *trans* to the phosphino group in ***trans*-Cl** easily dissociates to afford *trans*(*P*,*L*)-$[Ru(trpy)(Pqn)(L)]^{2+}$ due to the *trans*-labilizing effect.[28] The chloro ligand of $[Ru(trpy)(dppbz)Cl]^+$ was more labile than that of ***cis*-Cl**, allowing the transformation of $[Ru(trpy)(dppbz)Cl]^+$ to **PP** in acetonitrile without addition of silver ion (Ag^+). The *trans*-labilizing effect also explains the difference in ligand substitution rates of ***cis*-PN** and ***trans*-PN**; ***trans*-PN** immediately converted to ***trans*-PN^{DMF}** in DMF at room temperature, whereas the structure of ***cis*-PN** was preserved under the same conditions (Figures S11 and S12, Supporting Information).

In contrast, the π-acceptor character of phosphines stabilizes the energy levels of the dπ orbitals of the ruthenium center. As the number of phosphine donors increases, the dπ orbitals are more stabilized. Indeed, the oxidation potential of Ru(III)/Ru(II) for **PP** is higher than those of ***trans*-PN** and ***cis*-PN**, while that of **NN** is the lowest (Figure 5a). The blue shifts observed in the UV−vis absorption spectra upon introduction of phosphine moieties (Figure 4) also can be explained by stabilization of the dπ orbitals of the ruthenium center. These observations are supported by DFT and TD-DFT calculations (Figure 7 and Figure S9 (Supporting Information)) and are consistent with the results reported for the series $[Ru(bpy)_2(BL)](PF_6)_2$ (see Table 1).[29]

The difference in the stabilization of the dπ orbitals between ***trans*-PN** and ***cis*-PN** can be explained by considering interactions with the π* orbitals of trpy, Pqn, and acetonitrile ligands, as well as σ* orbitals of the P−C bonds of Pqn. The σ* orbitals of the P−C bonds can interact with two of the three dπ orbitals (d_{yz} and d_{zx} orbitals, with the Ru−P bond along the *z* axis). For both ***trans*-PN** and ***cis*-PN**, the two dπ orbitals stabilized by π back-bonding of the phosphine compose HOMO−2 and HOMO−1 (Scheme 5a and Figure S8 (Supporting Information)). As a result, the remaining dπ orbital without contribution from the π back-bonding of phosphine forms the HOMO. The HOMO of ***trans*-PN** lies in plane with the trpy ligand and can interact only with the π* orbitals of the quinoline moiety of Pqn. In contrast, that of ***cis*-PN** lies perpendicular to the trpy ligand and quinolone moiety

Scheme 5. (a) Two of the Three dπ Orbitals Stabilized by π-Back-Donation of a Phosphine and (b) HOMOs of *trans*-PN and *cis*-PN[a]

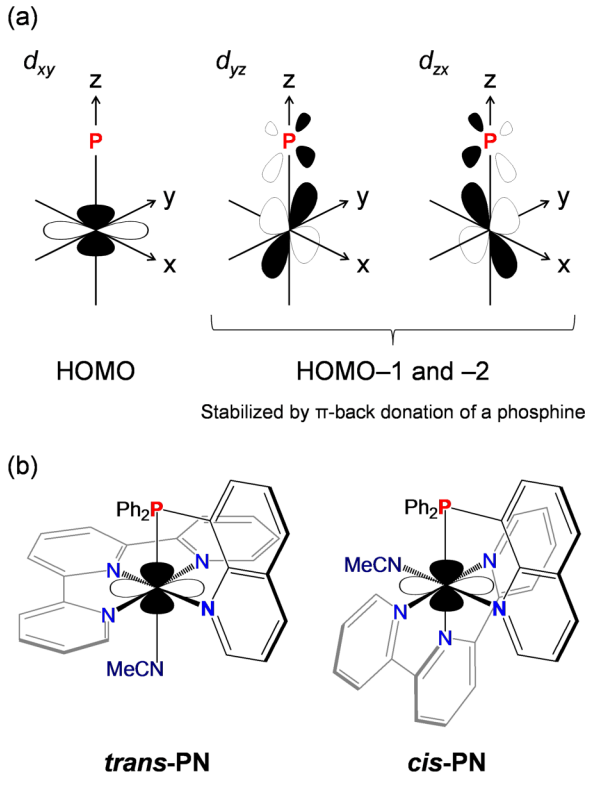

[a]The HOMO of ***trans*-PN** lies in plane with the trpy ligand and can interact only with π* orbitals of the quinoline moiety of Pqn. The HOMO of ***cis*-PN** lies perpendicular to the trpy ligand and the quinolone moiety of Pqn and thus is stabilized by the π* orbitals of trpy, Pqn, and MeCN.

dx.doi.org/10.1021/ic5003644 | *Inorg. Chem.* 2014, 53, 7214−7226

of Pqn and thus is stabilized by the π^* orbitals of trpy, Pqn, and acetonitrile ligands (Scheme 5b and Figure S8). Therefore, the HOMO of ***cis*-PN** was stabilized to a greater extent than that of ***trans*-PN**, resulting in a positive shift of the Ru(III)/Ru(II) potential and a blue shift of the MLCT band (Figures 4 and 5a).

Mechanism of Isomerization and Electrochemical Behavior. Although the results of X-ray crystallography, UV−vis absorption spectroscopy, and CVs in the positive potential region can be understood on the basis of σ donation and π back-donation of phosphine donors, the CVs of phosphine-containing complexes in the negative potential region exhibited behavior distinct from each other. Reduction of ***cis*-PN** led to *cis*−*trans* isomerization (Figure 6), and that of **PP** went through a two-electron transfer (Figure 5b). The mechanism of these various electrochemical behaviors is discussed in combination with *cis*−*trans* transformation behavior of ***cis*-PN** by heating or photoirradiation.

The *cis*−*trans* transformation proceeded upon moderate heating in DMF (Figure 8) and via visible-light irradiation (Figure 10). The positive values of $\Delta S^{\ddagger}$ and $\Delta H^{\ddagger}$ for solvent-induced isomerization in DMF indicate that the isomerization proceeds via a short-lived intermediate, $[Ru(trpy)(Pqn)]^{2+}$, after dissociation of the acetonitrile ligand (Scheme 6, top). Photochemical isomerization also can be explained by ligand dissociation from the ^{3}MC excited state to produce the short-lived five-coordinated species (Scheme 6, middle).[10d]

Scheme 6. Three Paths for Isomerization from *cis*-PN to *trans*-PN: (Top) Solvent-Induced Isomerization; (Middle) Photoinduced Isomerization; (Bottom) Reduction-Induced Isomerization[a]

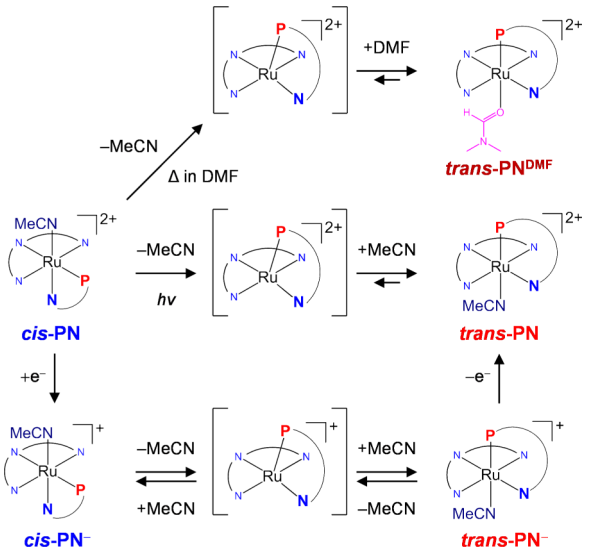

[a]All isomerization reactions from *cis* to *trans* proceed though the short-lived intermediates.

The concept of the five-coordinated species also can be used to explain the two-electron-transfer process of **PP** (Figure 5b) and the reduction-induced *cis*−*trans* isomerization of ***cis*-PN** (Figure 6). The two-electron process of **PP** implies that the reduction potential for **PP** lies at a potential more negative than that for the one-electron-reduced species of **PP**. Similar electrochemical behavior was reported for a ruthenium arene complex, $[Ru(\eta^6\text{-}C_6Me_6)(bpy)(MeCN)]^{2+}$, for which the acetonitrile ligand was lost upon electrochemical reduction of $[Ru(\eta^6\text{-}C_6Me_6)(bpy)(MeCN)]^{2+}$. $[Ru(\eta^6\text{-}C_6Me_6)(bpy)]^0$ was assumed to be the dominant form of the doubly reduced species.[13] On the basis of comparisons with the ruthenium arene complex, the two-electron reduction of **PP** may involve the five-coordinated doubly reduced species $[Ru(trpy)(dppbz)]^0$.

To discuss the electrochemical behaviors of ***cis*-PN** and **PP** in conjunction with five-coordinated species, bond dissociation free energies (BDFEs) upon liberation of the acetonitrile ligand were estimated. Table 2 shows BDFEs for the one-electron-reduced species of ***trans*-PN**, ***cis*-PN**, and **PP** (***trans*-PN**$^-$, ***cis*-PN**$^-$, and **PP**$^-$, determined by DFT calculations. The negative BDFEs suggest that dissociation of the acetonitrile ligand is favored in the equilibrium. Therefore, ligand dissociations are favored for ***cis*-PN**$^-$ and **PP**$^-$ (reactions 2 and 3, respectively, in Table 2), while dissociation is not favored for ***trans*-PN**$^-$ (reaction 1). In particular, the large negative ΔG° value for **PP**$^-$ implies that the equilibrium is largely shifted toward formation of the five-coordinated species $[Ru(trpy)(dppbz)]^+$ (reaction 3). The reduction potential for $[Ru(trpy)(dppbz)]^+/[Ru(trpy)(dppbz)]^0$ may be more positive than that for $[Ru(trpy)(dppbz)(MeCN)]^{2+}/[Ru(trpy)(dppbz)(MeCN)]^+$, leading to the two-electron process.[13,42] The generation of $[Ru(trpy)(dppbz)]^0$ upon reduction is also supported by the BDFE (reaction 4). For ***cis*-PN**, one-electron reduction may lead to ligand dissociation to give the five-coordinated species $[Ru(trpy)(Pqn)]^+$ ($\Delta G^\circ < 0$, for reaction 2), followed by rapid coordination of an acetonitrile molecule to the five-coordinated species to afford ***trans*-PN**$^-$ ($\Delta G^\circ > 0$, for reaction 1). Thus, the equilibrium of ***cis*-PN**$^-$, ***trans*-PN**$^-$, and $[Ru(trpy)(Pqn)]^+$ seems to be shifted toward ***trans*-PN**$^-$ to some extent, although the $|\Delta G^\circ|$ values are too small to explain the fact that only ***trans*-PN** was formed by the reoxidation of the equilibrium mixture (Figure 6). A reasonable explanation of the irreversible *cis*−*trans* conversion is given by considering the first reduction potentials of ***cis*-PN** ($E_{pc} \approx -1.6$ V) and ***trans*-PN** ($E^{\circ\prime}_1 = -1.70$ V). In the potential region between these two potentials ($E \approx -1.6$ to -1.7 V), ***cis*-PN** is reduced to ***cis*-PN**$^-$ and the generated ***cis*-PN**$^-$ reaches equilibrium with ***trans*-PN**$^-$ and $[Ru(trpy)(Pqn)]^+$. Then, ***trans*-PN**$^-$ in the equilibrium mixture can be oxidized to ***trans*-PN** in the same potential region (for a detailed explanation, see Scheme S1 in the Supporting

Table 2. Bond Dissociation Free Energies (BDFEs) for the One-Electron-Reduced Species of *trans*-PN, *cis*-PN, and PP (*trans*-PN$^-$, *cis*-PN$^-$, and PP$^-$, Respectively), and Two-Electron-Reduced Species of PP (PP^{2-}) Estimated by DFT Calculations[a]

reaction	ΔG° (kJ/mol)
One-Electron Reduction	
trans(P,MeCN)-$[Ru(trpy)(Pqn)(MeCN)]^+ \rightarrow [Ru(trpy)(Pqn)]^+ + MeCN$ (1)	2.5
cis(P,MeCN)-$[Ru(trpy)(Pqn)(MeCN)]^+ \rightarrow [Ru(trpy)(Pqn)]^+ + MeCN$ (2)	−1.4
$[Ru(trpy)(dppbz)(MeCN)]^+ \rightarrow [Ru(trpy)(dppbz)]^+ + MeCN$ (3)	−45.3
Two-Electron Reduction	
$[Ru(trpy)(dppbz)(MeCN)]^0 \rightarrow [Ru(trpy)(dppbz)]^0 + MeCN$ (4)	−19.3

[a]See also Table S6 (Supporting Information).

dx.doi.org/10.1021/ic5003644 | *Inorg. Chem.* 2014, 53, 7214−7226

Information). Therefore, the potential sweeping over $E \approx -1.6$ to -1.7 V results in the irreversible conversion from ***cis*-PN** to ***trans*-PN** via the five-coordinated species (Scheme 6, bottom).

CONCLUSION

This study describes the effects of the substitution of phosphines for pyridine in a series of ruthenium(II) polypyridine complexes with a monodentate labile ligand. The structures and electronic properties of ruthenium(II) complexes were expected to be systematically controlled by the number and position of the phosphines. Indeed, the σ-donating and π-accepting character of the phosphines clearly influenced the dσ and dπ orbitals of the metal center, respectively, which was supported by crystallographic, spectroscopic, and electrochemical analyses. Furthermore, electrochemical behaviors of these complexes in their reduction reactions were totally different among them. The mechanisms explaining these results were elucidated by considering five-coordinated species formed via liberation of the monodentate labile ligand. These results are significant because they show a clear relation between the redox properties of the metal complexes and the liberation of a labile ligand and therefore provide important information for the development of new catalysts for electrochemical and photochemical reactions.

EXPERIMENTAL SECTION

General Methods. The ^{1}H and ^{31}P{^{1}H} NMR spectra were recorded at room temperature on a JEOL JNM-LA500 spectrometer using tetramethylsilane as an internal reference for ^{1}H NMR spectra and phosphoric acid as an external reference for ^{31}P{^{1}H} NMR spectra. UV−vis absorption spectra were obtained on a Shimadzu UV-2450SIM spectrophotometer at room temperature. Elemental analyses were conducted on a J-Science Lab Micro Corder JM10 elemental analyzer. ESI-TOF mass spectra were recorded on a JEOL JMS-T100LC mass spectrometer. All of the ESI-TOF mass spectrometric measurements were obtained in the positive ion mode at a cone voltage of 20 V. Typically, each sample solution was introduced into the spectrometer at a flow rate of 10 mL min^{-1} using a syringe pump. Cyclic voltammograms were measured at room temperature on a BAS ALS Model 650DKMP electrochemical analyzer in acetonitrile ([complex] = 0.5 mM; 0.1 M tetraethylammonium perchlorate (TEAP)). A glassy-carbon disk, platinum wire, and Ag/Ag$^+$ electrode (Ag/0.01 M $AgNO_3$) were used as the working, auxiliary, and reference electrodes, respectively. The redox potentials of samples were calibrated against the redox signal for the ferrocene/ferrocenium (Fc/Fc$^+$) couple. The photoisomerization was performed using a 150 W xenon lamp (CX-04E, Eagle Engineering) as a probe with a cut filter (λ >370 nm). Global kinetic analysis was conducted using the singular value decomposition (SVD) method in SPECFIT,[36] in the range 300−600 nm. The amount of O_2 evolved was monitored using a YSI Model 5300A oxygen meter at room temperature under an Ar atmosphere.[9a]

Materials. Pqn [8-(diphenylphosphanyl)quinoline],[43] [$RuCl_3$(trpy)]·H_2O (trpy = 2,2′:6′,2″-terpyridine),[27] and [Ru(trpy)(bpy)(MeCN)]$(PF_6)_2$ (**NN**)[25] were prepared by methods reported previously. dppbz (1,2-bis(diphenylphosphanyl)benzene) and $NaPF_6$ were purchased from Wako Pure Chemical Industries, Ltd. $AgPF_6$ was purchased from Sigma-Aldrich Co. All solvents and reagents were of the highest quality available and were used as received.

Synthesis of *cis(P,Cl)*-[Ru(trpy)(Pqn)Cl]PF_6 (*cis*-Cl). A mixture of [$RuCl_3$(trpy)]·H_2O (94.0 mg, 0.205 mmol), Pqn (64.6 mg, 0.206 mmol), and ascorbic acid (68.7 mg, 0.390 mmol) in ethanol (100 cm^3) was refluxed for 4 h and then cooled to room temperature. The solution was filtered and the purple filtrate concentrated to ca. 5 cm^3 under reduced pressure. A saturated $NaPF_6$/water solution was added to the solution under refrigeration, resulting in a purple precipitate. The crude product was further purified by gel permeation chromatography (Sephadex LH-20) using an acetonitrile/methanol (1/1) mixture as the eluent. The product was recrystallized from dichloromethane and a small amount of acetonitrile/diethyl ether to yield deep purple crystals of ***cis*-Cl** (0.089 mmol, 43%). ESI-TOF MS (positive ion, acetonitrile): m/z 683 ([Ru(trpy)(Pqn)Cl]$^+$). ^{1}H NMR (CD_3CN): δ 6.70 (t, 2H, J = 6.5 Hz), 6.95 (t, 1H, J = 8.5 Hz), 7.38 (d, 2H, J = 6.0 Hz), 7.50 (t, 4H, J = 7.0 Hz), 7.57 (t, 2H, J = 7.5 Hz), 7.75 (t, 2H, J = 7.5 Hz), 8.08 (m, 7H), 8.20 (d, 1H, J = 9.0 Hz), 8.30 (t, 1H, J = 7.5 Hz), 8.35 (d, 2H, J = 8.0 Hz), 8.56 (d, 2H, J = 8.5 Hz), 9.01 (t, 1H, J = 7.5 Hz). ^{31}P{^{1}H} NMR (CD_3CN): δ 51.16 (s). Anal. Found: C, 50.52; H, 3.44; N, 6.54. Calcd for $C_{36.5}H_{28}F_6Cl_2N_4P_2Ru$ (***cis*-Cl**·0.5CH_2Cl_2): C, 50.36; H, 3.24; N, 6.44.

Synthesis of *cis(P,Cl)*-[Ru(trpy)(Pqn)Cl]BPh_4 (*cis*-Cl′). This complex was prepared by counterion exchange of ***cis*-Cl** (16.9 mg, 0.0194 mmol) with excess $NaBPh_4$. The product was recrystallized from dichloromethane and a small amount of acetonitrile/diethyl ether to afford purple crystals of ***cis*-Cl′** (0.0124 mmol, 64%). Anal. Found: C, 71.72; H, 4.74; N, 5.59. Calcd for $C_{60}H_{47}BClN_4PRu$ (***cis*-Cl′**): C, 71.90; H, 4.73; N, 5.59.

Synthesis of *trans(P,MeCN)*-[Ru(trpy)(Pqn)(MeCN)]$(PF_6)_2$ (*trans*-PN). A mixture of ***cis*-Cl** (108 mg, 0.124 mmol) and $AgPF_6$ (34.8 mg, 0.138 mmol) in 2-butanone (10 cm^3)/water (5 cm^3) was heated to 100 °C for 1 day. The resulting red solution was evaporated to dryness under reduced pressure. The residue was extracted with a small amount of acetonitrile, and the precipitate of AgCl was removed by filtration. The product was recrystallized from dichloromethane and a few drops of acetonitrile/diethyl ether to afford orange crystals of ***trans*-PN** (0.102 mmol, 82%). ESI-TOF MS (positive ion, acetonitrile): m/z 324 ([Ru(trpy)(Pqn)]$^{2+}$), 345 ([Ru(trpy)(Pqn)(MeCN)]$^{2+}$). ^{1}H NMR (CD_3CN): δ 6.59 (t, 4H, J = 8.5 Hz), 6.99 (t, 4H, J = 7.5 Hz), 7.15 (d, 2H, J = 6.5 Hz), 7.24 (t, 2H, J = 7.5 Hz), 7.57 (t, 2H, J = 6.0 Hz), 7.84 (t, 2H, J = 8.5 Hz), 7.96 (m, 3H), 8.07 (d, 2H, J = 9.0 Hz), 8.22 (t, 1H, J = 7.5 Hz), 8.32 (d, 2H, J = 8.0 Hz), 8.52 (d, 1H, J = 7.5 Hz), 8.83 (d, 1H, J = 8.0 Hz), 9.85 (d, 1H, J = 7.5 Hz). ^{31}P{^{1}H} NMR (CD_3CN): δ 58.80 (s). Anal. Found: C, 44.12; H, 3.24; N, 6.59. Calcd for $C_{39}H_{32}F_{12}Cl_2N_5P_3Ru$ (***trans*-PN**·CH_2Cl_2): C, 44.04; H, 3.03; N, 6.58.

Synthesis of *cis(P,MeCN)*-[Ru(trpy)(Pqn)(MeCN)]$(PF_6)_2$ (*cis*-PN). A mixture of ***cis*-Cl** (85.1 mg, 0.103 mmol) and $AgPF_6$ (28.0 mg, 0.111 mmol) in acetonitrile (15 cm^3) was heated to 70 °C for 2 days and then cooled to room temperature. The resulting orange solution was evaporated to dryness under reduced pressure. The residue was extracted with a small amount of acetonitrile, and the precipitate of AgCl was removed by filtration. The product was recrystallized from chloroform and a few drops of acetonitrile/diethyl ether to afford orange crystals of ***cis*-PN** (0.096 mmol, 93%). ESI-TOF MS (positive ion, acetonitrile): m/z 324 ([Ru(trpy)(Pqn)]$^{2+}$), 345 ([Ru(trpy)(Pqn)(MeCN)]$^{2+}$). ^{1}H NMR (CD_3CN): δ 6.83 (t, 2H, J = 6.5 Hz), 7.10 (d, 1H, J = 8.0 Hz), 7.26 (d, 2H, J = 6.5 Hz), 7.57 (t, 4H, J = 7.0 Hz), 7.67 (t, 2H, J = 7.5 Hz), 7.77 (d, 2H, J = 8.0 Hz), 7.79 (d, 2H, J = 8.0 Hz), 7.89 (t, 2H, J = 8.0 Hz), 7.97 (d, 1H, J = 5.5 Hz), 8.04 (t, 1H, J = 7.5 Hz), 8.24 (d, 1H, J = 8.0 Hz), 8.28 (d, 1H, J = 8.0 Hz), 8.41 (d, 2H, J = 8.0 Hz), 8.50 (t, 1H, J = 8.0 Hz), 8.65 (d, 2H, J = 8.0 Hz), 8.89 (t, 1H, J = 8.0 Hz). ^{31}P{^{1}H} NMR (CD_3CN): δ 55.96 (s). Anal. Found: C, 44.38; H, 3.13; N, 6.73. Calcd for $C_{38.5}H_{31}Cl_{1.5}N_5P_3Ru$ (***cis*-PN**·0.5$CHCl_3$): C, 44.53; H, 2.96; N, 6.74.

Synthesis of [Ru(trpy)(dppbz)(MeCN)]$(PF_6)_2$ (PP). A mixture of [$RuCl_3$(trpy)]·H_2O (62.0 mg, 0.135 mmol), dppbz (63.1 mg, 0.141 mmol), and ascorbic acid (52.3 mg, 0.297 mmol) in ethanol (50 cm^3) was refluxed for 4 h and then cooled to room temperature. The solution was filtered and the purple filtrate concentrated to ca. 5 cm^3 under reduced pressure. A saturated $NaPF_6$/water solution was added to the solution under refrigeration, which resulted in a purple precipitate. Purification of the crude product by gel permeation chromatography (Sephadex LH-20) using an acetonitrile/methanol (1/1) mixture as the eluent produced an orange band followed by a purple band of *cis(MeCN,MeCN)*-[Ru(trpy)$(MeCN)_2$Cl]PF_6 (**trpyMeCN2Cl**) (see the synthesis of **trpyMeCN2Cl** in the Supporting Information). The orange solution was evaporated, and a saturated $NaPF_6$/acetonitrile solution (30 cm^3) was added to the residue. The

dx.doi.org/10.1021/ic5003644 | Inorg. Chem. 2014, 53, 7214−7226

mixture was refluxed for 3 h, cooled to room temperature, and then evaporated to dryness under reduced pressure. The residue was extracted with dichloromethane, and the salts were removed by filtration. After evaporation of the solvent, the dried solid was dissolved in a minimum amount of dichloromethane and then loaded onto a silica gel column. The column was eluted with dichloromethane/acetonitrile (9/1) to give an orange band followed by a yellow band. **PP** was obtained from the yellow band after evaporation and recrystallization from a dichloromethane/acetonitrile mixture (1/1) and diethyl ether as yellow crystals (0.034 mmol, 25%). ESI-TOF MS (positive ion, acetonitrile): m/z 391 ($[Ru(trpy)(dppbz)]^{2+}$), 411 ($[Ru(trpy)(dppbz)(MeCN)]^{2+}$). ^{1}H NMR ($CD_3CN$): 6.56 (t, 4H, J = 8.0 Hz), 6.76 (t, 2H, J = 5.5 Hz), 6.83 (d, 2H, J = 6.0 Hz), 6.91 (t, 4H, J = 8.0 Hz), 7.20 (t, 2H, J = 7.5 Hz), 7.51 (t, 4H, J = 8.0 Hz), 7.63 (m, 6H), 7.70 (t, 1H, J = 8.0 Hz), 7.82 (m, 3H), 7.99 (t, 1H, J = 7.5 Hz), 8.09 (d, 2H, J = 8.5 Hz), 8.37 (m, 3H), 8.53 (t, 1H, J = Hz). ^{31}P{^{1}H} NMR (CD_3CN): δ 68.57 (d, $^2J_{P-P}$ = 20.2 Hz), 69.77 (d, $^2J_{P-P}$ = 20.2 Hz). Anal. Found: C, 48.32; H, 3.52; N, 4.81. Calcd for $C_{48}H_{40}F_{12}Cl_2N_4P_4Ru$ (**PP**·CH_2Cl_2): C, 48.17; H, 3.37; N, 4.68.

Crystallography. Diffraction data at 123 K were obtained using a Rigaku AFC8 diffractometer with a Rigaku Saturn CCD system. Graphite-monochromated Mo Kα radiation (0.71075 Å) was used. Cell parameters were retrieved using Crystal Clear-SM 1.4.0 software and refined using Crystal Clear-SM 1.4.0 on all observed reflections. Data reduction and empirical absorption correction using equivalent reflections and Lorentzian polarization were performed with the Crystal Clear-SM 1.4.0 software. The structure was solved by direct methods using SIR-92[44]and refined on F^2 with the full-matrix least-squares technique using SHELXL-97.[45] All non-hydrogen atoms were refined anisotropically. Molecular graphics were generated using ORTEP-3 for Windows[46] and POV-RAY.[47] For ***cis*-PN**, the diffused electron densities resulting from residual solvent molecules were removed from the data set using the SQUEEZE routine of PLATON and refined further using the data generated.

Crystallographic data have been deposited with Cambridge Crystallographic Data Center: deposition numbers CCDC 971295, 971296, 971297, and 971298 for ***cis*-Cl′**, ***trans*-PN**, ***cis*-PN**, and **PP**, respectively. Copies of the data can be obtained free of charge via www.ccdc.cam.ac.uk/data_request/cif.

DFT Calculations. Calculations were performed using the DFT method implemented in the Gaussian 09 package of programs.[33] The structures were fully optimized using the B3LYP method, which uses hybrid Becke's three-parameter exchange functional[34] with the correlation energy functional of Lee, Yang, and Parr.[35] All calculations were performed using the standard double-ζ type LanL2DZ basis set[36] implemented in Gaussian 09, without adding any extra polarization or diffuse function. The LanL2DZ basis set also uses relativistic effective core potentials (RECP) for the Ru atom to account for the scalar relativistic effects of the inner 28 core electrons ($[Ar]3d^{10}$) for Ru. All calculations were performed using the polarizable continuum model (PCM)[37] to compute the structures in acetonitrile. All stationary points were characterized by their harmonic vibrational frequencies as minima. The free energies at 298 K and 1 atm were obtained through thermochemical analysis of the frequency calculation, using the thermal correction to Gibbs free energy as reported by Gaussian 09. The excited states were calculated using the TD-DFT[38] method within the Tamm−Dancoff approximation as implemented in Gaussian 09. These calculations employ the hybrid B3LYP functional along with the basis sets described above. At least 100 excited states were computed in each calculation. To obtain the simulated spectrum of each species, transition energies and oscillator strengths have been interpolated by a Gaussian convolution with a common σ value of 0.2 eV.

■ ASSOCIATED CONTENT

Supporting Information

Text, tables, figures, and CIF files giving detailed X-ray crystallographic parameters for ***cis*-Cl′**, ***trans*-PN**, ***cis*-PN**, and **PP**, and additional data for DFT calculations, ^{1}H NMR, and electrochemistry. This material is available free of charge via the Internet at http://pubs.acs.org.

■ AUTHOR INFORMATION

Corresponding Author

*E-mail for S.M.: masaoka@ims.ac.jp.

Present Address

$^{\$}$Department of Chemistry, Faculty of Science, Hokkaido University, North-10 West-8, Kita-ku, Sapporo 060-0810, Japan.

Notes

The authors declare no competing financial interest.

■ ACKNOWLEDGMENTS

This study was supported by Grants-in-Aid for Young Scientists A (No. 25708011) and for Challenging Exploratory Research (No. 24655135) from the Japan Society for the Promotion of Science (to S.M.), a Grant-in-Aid for Scientific Research in Innovative Areas (No. 25107526) from the Ministry of Education, Culture, Sports, Science, and Technology (to S.M.), a Grant-in-Aid for Young Scientists B (No. 24750140) from the Japan Society for the Promotion of Science (to M.K.), a Shiseido Female Researcher Science Grant from Shiseido Co. Ltd. (to M.K.), and the NINS Program for Cross-Disciplinary Study. The computations were performed at the Research Center for Computational Science, Okazaki, Japan.

■ REFERENCES

(1) (a) Kalyanasundaram, K. *Coord. Chem. Rev.* **1982**, *46*, 159−244. (b) Juris, A.; Balzani, V.; Barigelletti, F.; Campagna, S.; Belser, P.; von Zelewsky, A. *Coord. Chem. Rev.* **1988**, *84*, 85−277.

(2) (a) Sutin, N. *J. Photochem.* **1979**, *10*, 19−40. (b) Dodsworth, E. S.; Lever, A. B. P. *Chem. Phys. Lett.* **1986**, *124*, 152−158. (c) Lever, A. B. P. *Inorg. Chem.* **1990**, *29*, 1271−1285. (d) Thompson, D. W.; Wishart, J. F.; Brunschwig, B. S.; Sutin, N. *J. Phys. Chem. A* **2001**, *105*, 8117−8122.

(3) (a) Clark, C. D.; Hoffman, M. Z. *Coord. Chem. Rev.* **1997**, *159*, 359−373. (b) De Cola, L.; Belser, P. *Coord. Chem. Rev.* **1998**, *177*, 301−346. (c) Ward, M. D.; Barigelletti, F. *Coord. Chem. Rev.* **2001**, *216−217*, 127−154.

(4) (a) Beer, P. D. *Acc. Chem. Res.* **1998**, *31*, 71−80. (b) Wu, A.; Yoo, D.; Lee, J.-K.; Rubner, M. F. *J. Am. Chem. Soc.* **1999**, *121*, 4883−4891. (c) Gao, F. G.; Bard, A. J. *J. Am. Chem. Soc.* **2000**, *122*, 7426−7427. (d) Demas, J. N.; DeGraff, B. A. *Coord. Chem. Rev.* **2001**, *211*, 317−351. (e) Polo, A. S.; Itokazu, M. K.; Iha, N. Y. M. *Coord. Chem. Rev.* **2004**, *248*, 1343−1361.

(5) (a) Wilson, G. J.; Launikonis, A.; Sasse, W. H. F.; Mau, A. W.-H. *J. Phys. Chem. A* **1997**, *101*, 4860−4866. (b) Simon, J. A.; Curry, S. L.; Schmehl, R. H.; Schatz, T. R.; Piotrowiak, P.; Jin, X.; Thummel, R. P. *J. Am. Chem. Soc.* **1997**, *119*, 11012−11022. (c) Tyson, D. S.; Luman, C. R.; Zhou, X.; Castellano, F. N. *Inorg. Chem.* **2001**, *40*, 4063−4071. (d) Guerzo, A. D.; Leroy, S.; Fages, F.; Schmehl, R. H. *Inorg. Chem.* **2002**, *41*, 359−366.

(6) (a) Barton, J. K. *Science* **1986**, *233*, 727−734. (b) Turro, C.; Bossmann, S. H.; Jenkins, Y.; Barton, J. K.; Turro, N. J. *J. Am. Chem. Soc.* **1995**, *117*, 9026−9032. (c) Gray, H. B.; Winkler, J. R. *Annu. Rev. Biochem.* **1996**, *65*, 537−561. (d) Guerzo, A. D.; Mesmaeker, A. K.-D. *Inorg. Chem.* **2002**, *41*, 938−945.

(7) (a) Meyer, T. J.; Huynh, M. H. V. *Inorg. Chem.* **2003**, *42*, 8140−8160. (b) Masllorens, E.; Rodriguez, M.; Romero, I.; Roglans, A.; Parella, T.; Benet-Buchholz, J.; Poyatos, M.; Llobet, A. *J. Am. Chem. Soc.* **2006**, *128*, 5306−5307.

(8) (a) Concepcion, J. J.; Jurss, J. W.; Templeton, J. L.; Meyer, T. J. *J. Am. Chem. Soc.* **2008**, *130*, 16462−16463. (b) Tseng, H.-W.; Zong, R.; Muckerman, J. T.; Thummel, R. P. *Inorg. Chem.* **2008**, *47*, 11763−

11773. (c) Romain, S.; Vigara, L.; Llobet, A. *Acc. Chem. Res.* **2009**, *42*, 1944−1953. (d) Concepcion, J. J.; Jurss, J. W.; Brennaman, M. K.; Hoertz, P. G.; Patrocinio, A. O. T.; Murakami Iha, N. Y.; Templeton, J. L.; Meyer, T. J. *Acc. Chem. Res.* **2009**, *42*, 1954−1965. (e) Duan, L.; Tong, L.; Xu, Y.; Sun, L. *Energy Environ. Sci.* **2011**, *4*, 3296−3313. (f) Wasylenko, D. J.; Palmer, R. D.; Berlinguette, C. P. *Chem. Commun.* **2013**, *49*, 218−227.

(9) (a) Masaoka, S.; Sakai, K. *Chem. Lett.* **2009**, *38*, 182−183. (b) Yoshida, M.; Masaoka, S.; Sakai, K. *Chem. Lett.* **2009**, *38*, 702−703. (c) Yoshida, M.; Masaoka, S.; Abe, J.; Sakai, K. *Chem. Asian J.* **2010**, *5*, 2369−2378. (d) Kiyota, J.; Yokoyama, J.; Yoshida, M.; Masaoka, S.; Sakai, K. *Chem. Lett.* **2010**, *39*, 1146−1148. (e) Kimoto, A.; Yamauchi, K.; Yoshida, M.; Masaoka, S.; Sakai, K. *Chem. Commun.* **2012**, *48*, 239−241. (f) Okamura, M.; Yoshida, M.; Kuga, R.; Sakai, K.; Kondo, M.; Masaoka, S. *Dalton Trans.* **2012**, *41*, 13081−13089.

(10) (a) Yamazaki, H.; Hakamata, T.; Komi, M.; Yagi, M. *J. Am. Chem. Soc.* **2011**, *133*, 8846−8849. (b) Boyer, J. L.; Polyansky, D. E.; Szalda, D. J.; Zong, R.; Thummel, R. P.; Fujita, E. *Angew. Chem., Int. Ed.* **2011**, *50*, 12600−12604. (c) Padhi, S. K.; Fukuda, R.; Ehara, M.; Tanaka, K. *Inorg. Chem.* **2012**, *51*, 5386−5392. (d) Hirahara, M.; M. Ertem, Z.; Komi, M.; Yamazaki, H.; Cramer, C. J.; Yagi, M. *Inorg. Chem.* **2013**, *52*, 6354−6364.

(11) (a) Nagao, H.; Mizukawa, T.; Tanaka, K. *Chem. Lett.* **1993**, *22*, 955−958. (b) Nakajima, H.; Kushi, Y.; Nagao, H.; Tanaka, K. *Organometallics* **1995**, *14*, 5093−5098. (c) Tanaka, K.; Ooyama, D. *Coord. Chem. Rev.* **2002**, *226*, 211−218. (d) Savéant, J.-M. *Chem. Rev.* **2008**, *108*, 2348−2378.

(12) Chen, Z.; Chen, C.; Weinberg, D. R.; Kang, P.; Concepcion, J. J.; Harrison, D. P.; Brookhart, M. S.; Meyer, T. J. *Chem. Commun.* **2011**, *47*, 12607−12609.

(13) Matsubara, Y.; Fujita, E.; Doherty, M. D.; Muckerman, J. T.; Creutz, C. *J. Am. Chem. Soc.* **2012**, *134*, 15743−15757.

(14) (a) Kobayashi, A.; Takatori, R.; Kikuchi, I.; Konno, H.; Sakamoto, K.; Ishitani, O. *Organometallics* **2001**, *20*, 3361−3363. (b) Kobayashi, A.; Konno, H.; Sakamoto, K.; Sekine, A.; Ohashi, Y.; Iida, M.; Ishitani, O. *Chem. Eur. J.* **2005**, *11*, 4219−4226. (c) Koizumi, T.; Tanaka, K. *Angew. Chem., Int. Ed.* **2005**, *44*, 5891−5894. (d) Polyansky, D.; Cabelli, D.; Muckerman, J. T.; Fujita, E.; Koizumi, T.; Fukushima, T.; Wada, T.; Tanaka, K. *Angew. Chem., Int. Ed.* **2007**, *46*, 4169−4172. (e) Tannai, H.; Koizumi, T.; Wada, T.; Tanaka, K. *Angew. Chem., Int. Ed.* **2007**, *46*, 7112−7115. (f) Kimura, M.; Tanaka, K. *Angew. Chem., Int. Ed.* **2008**, *47*, 9768−9771. (g) Polyansky, D. E.; Cabelli, D.; Muckerman, J. T.; Fukushima, T.; Tanaka, K.; Fujita, E. *Inorg. Chem.* **2008**, *47*, 3958−3968. (h) Fukushima, T.; Fujita, E.; Muckerman, J. T.; Polyansky, D. E.; Wada, T.; Tanaka, K. *Inorg. Chem.* **2009**, *48*, 11510−11512. (i) Matsubara, Y.; Koga, K.; Kobayashi, A.; Konno, H.; Sakamoto, K.; Morimoto, T.; Ishitani, O. *J. Am. Chem. Soc.* **2010**, *132*, 10547−10552. (j) Padhi, S. K.; Kobayashi, K.; Masuno, S.; Tanaka, K. *Inorg. Chem.* **2011**, *50*, 5321−5323.

(15) Kinoshita, T.; Dy, J. T.; Uchida, S.; Kubo, T.; Segawa, H. *Nat. Photonics* **2013**, *7*, 535−539.

(16) (a) Noyori, R.; Ohkuma, T. *Angew. Chem., Int. Ed.* **2001**, *40*, 40−73. (b) Noyori, R. *Angew. Chem., Int. Ed.* **2002**, *41*, 2008−2022.

(17) (a) Schwab, P.; France, M. B.; Ziller, J. W.; Grubbs, R. H. *Angew. Chem., Int. Ed.* **1995**, *34*, 2039−2041. (b) Vougioukalakis, G. C.; Grubbs, R. H. *Chem. Rev.* **2010**, *110*, 1746−1787. (c) Samec, J. S. M.; Keitz, B. K.; Grubbs, R. H. *J. Organomet. Chem.* **2010**, *695*, 1831−1837.

(18) (a) Clavier, H.; Nolan, S. P. *Chem. Eur. J.* **2007**, *13*, 8029−8036. (b) Nolan, S. P.; Clavier, H. *Chem. Soc. Rev.* **2010**, *39*, 3305−3316.

(19) (a) Dutta, D. K.; Deb, B. *Coord. Chem. Rev.* **2011**, *255*, 1686−1712. (b) Yi, C. S. *J. Organomet. Chem.* **2011**, *696*, 76−80. (c) Mellone, I.; Peruzzini, M.; Rosi, L.; Mellmann, D.; Junge, H.; Beller, M.; Gonsalvi, L. *Dalton Trans.* **2013**, *42*, 2495−2501.

(20) (a) Leising, R. A.; Grzybowski, J. J.; Takeuchi, K. J. *Inorg. Chem.* **1988**, *27*, 1020−1025. (b) Coe, B. J.; Thompson, D. W.; Culbertson, C. T.; Schoonover, J. R.; Meyer, T. J. *Inorg. Chem.* **1995**, *34*, 3385−3395. (c) Szczepura, L. F.; Kubow, S. A.; Leising, R. A.; Perez, W. J.; Huynh, M. H. V.; Lake, C. H.; Churchill, D. G.; Churchill, M. R.; Takeuchi, K. J. *J. Chem. Soc., Dalton Trans.* **1996**, *7*, 1463−1470. (d) Perez, W. J.; Lake, C. H.; See, R. F.; Toomey, L. M.; Churchill, M. R.; Takeuchi, K. J.; Radano, C. P.; Boyko, W. J.; Bessel, C. A. *J. Chem. Soc., Dalton Trans.* **1999**, 2281−2292. (e) Billings, S. B.; Mock, M. T.; Wiacek, K.; Turner, M. B.; Kassel, W. S.; Takeuchi, K. J.; Rheingold, A. L.; Boyko, W. J.; Bessel, C. A. *Inorg, Chim. Acta* **2003**, *355*, 103−115. (f) Sharma, S.; Singh, S. K.; Chandra, M.; Pandey, D. S. *J. Inorg. Biochem.* **2005**, *99*, 458−466. (g) Moore, C. M.; Szymczak, N. K. *Chem. Commun.* **2013**, *49*, 400−402.

(21) (a) Sullivan, B. P.; Salmon, D. J.; Meyer, T. J. *Inorg. Chem.* **1978**, *17*, 3334−3341. (b) Sullivan, B. P.; Conrad, D.; Meyer, T. J. *Inorg. Chem.* **1985**, *24*, 3640−3645. (c) Otruba, J. P.; Neyhart, G. A.; Dressick, W. J.; Marshall, J. L.; Sullivan, B. P.; Watkins, P. A.; Meyer, T. J. *J. Photochem.* **1986**, *35*, 133−153. (d) Leising, R. A.; Takeuchi, K. J. *Inorg. Chem.* **1987**, *26*, 4391−4393. (e) Leising, R. A.; Ohman, J. S.; Takeuchi, K. J. *Inorg. Chem.* **1988**, *27*, 3804−3809. (f) Bessel, C. A.; Margarucci, J. A.; Acquaye, J. H.; Rubmo, R. S.; Crandall, J.; Jircitano, A. J.; Takeuchi, K. J. *Inorg. Chem.* **1993**, *32*, 5779−5784. (g) Churchill, M. R.; Krajkowski, L. M.; Huynh, M. H. V.; Takeuchi, K. J. *J. Chem. Crystallogr.* **1997**, *27*, 589−597. (h) Salierno, M.; Marceca, E.; Peterka, D. S.; Yuste, R.; Etchenique, R. *J. Inorg. Biochem.* **2010**, *104*, 418−422. (i) Litke, S. V.; Ershov, A. Y.; Meyer, T. J. *J. Phys. Chem. A* **2011**, *115*, 14235−14242. (j) Miguel, V. S.; Aìlvarez, M.; Filevich, O.; Etchenique, R.; del Campo, A. *Langmuir* **2012**, *28*, 1217−1221. (k) Araya, R.; Andino-Pavlovsky, V.; Yuste, R.; Etchenique, R. *ACS Chem. Neurosci.* **2013**, *4*, 1163−1167.

(22) (a) Nikol'skii, A. B.; Egorova, M. B.; Repinskaya, T. S.; Gindin, V. A.; Popov, A. M. *Zh. Obshch. Khim.* **1986**, *56*, 2415−2416. (b) Sussuchi, E. M.; De Lima, A. A.; De Giovani, W. F. *Polyhedron* **2006**, *25*, 1457−1463. (c) Sinha, P.; Raghuvanshi, D. S.; Singh, K. N.; Mishra, L. *Polyhedron* **2012**, *31*, 227−234.

(23) (a) Hecker, C. R.; Fanwick, P. E.; McMillin, D. R. *Inorg. Chem.* **1991**, *30*, 659−666. (b) Tsai, C.-N.; Allard, M. M.; Lord, R. L.; Luo, D.-W.; Chen, Y.-J.; Schlegel, H. B.; Endicott, J. F. *Inorg. Chem.* **2011**, *50*, 11965−11977.

(24) Rasmussen, S. C.; Ronco, S. E.; Mlsna, D. A.; Billadeau, M. A.; Pennington, W. T.; Kolis, J. W.; Petersen, J. D. *Inorg. Chem.* **1995**, *34*, 821−829.

(25) Takeuchi, K. J.; Thompson, M. S.; Pipes, D. W.; Meyer, T. J. *Inorg. Chem.* **1984**, *23*, 1845−1851.

(26) Wehman, P.; van Donge, H. M. A.; Hagos, A.; Kamer, P. C. J.; van Leeuwen, P. W. N. M. *J. Organomet. Chem.* **1997**, *535*, 183−193.

(27) Sullivan, B. P.; Calver, J. M.; Meyer, T. J. *Inorg. Chem.* **1980**, *19*, 1404−1407.

(28) (a) Simándi, L. I.; Neméth, S. *Inorg. Chim. Acta* **1998**, *270*, 326−329. (b) Coe, B. J.; Glenwright, S. J. *Coord. Chem. Rev.* **2000**, *203*, 5−80. (c) Smithback, J. L.; Helms, J. B.; Schutte, E.; Woessner, S. M.; Sullivan, B. P. *Inorg. Chem.* **2006**, *45*, 2163−2174.

(29) (a) Suzuki, T.; Kuchiyama, T.; Kishi, S.; Kaizaki, S.; Kato, M. *Bull. Chem. Soc. Jpn.* **2002**, *75*, 2433−2439. (b) Suzuki, T.; Kuchiyama, T.; Kishi, S.; Kaizaki, S.; Takagi, H. D.; Kato, M. *Inorg. Chem.* **2003**, *42*, 785−795.

(30) (a) Suen, H.-F.; Wilson, S. W.; Pomerantz, M.; Walsh, J. L. *Inorg. Chem.* **1989**, *28*, 786−791. (b) Fanni, S.; Weldon, F. M.; Hammarstrom, L.; Mukhtar, E.; Browne, W. R.; Keyes, T. E.; Vos, J. G. *Eur. J. Inorg. Chem.* **2001**, *2*, 529−534.

(31) Taketoshi, A.; Koizumi, T.; Kanbara, T. *Tetrahedron Lett.* **2010**, *51*, 6457−6459.

(32) Wadman, S. H.; Lutz, M.; Tooke, D. M.; Spek, A. L.; Hartl, F.; Havenith, R. W. A.; van Klink, G. P. M.; van Koten, G. *Inorg. Chem.* **2009**, *48*, 1887−1900.

(33) Frisch, M. J.; Trucks, G. W.; Schlegel, H. B.; Scuseria, G. E.; Robb, M. A.; Cheeseman, J. R.; Scalmani, G.; Barone, V.; Mennucci, B.; Petersson, G. A.; Nakatsuji, H.; Caricato, M.; Li, X.; Hratchian, H. P.; Izmaylov, A. F.; Bloino, J.; Zheng, G.; Sonnenberg, J. L.; Hada, M.; Ehara, M.; Toyota, K.; Fukuda, R.; Hasegawa, J.; Ishida, M.; Nakajima, T.; Honda, Y.; Kitao, O.; Nakai, H.; Vreven, T.; Montgomery, J. A., Jr.; Peralta, J. E.; Ogliaro, F.; Bearpark, M.; Heyd, J. J.; Brothers, E.; Kudin,

K. N.; Staroverov, V. N.; Keith, T.; Kobayashi, R.; Normand, J.; Raghavachari, K.; Rendell, A.; Burant, J. C.; Iyengar, S. S.; Tomasi, J.; Cossi, M.; Rega, N.; Millam, J. M.; Klene, M.; Knox, J. E.; Cross, J. B.; Bakken, V.; Adamo, C.; Jaramillo, J.; Gomperts, R.; Stratmann, R. E.; Yazyev, O.; Austin, A. J.; Cammi, R.; Pomelli, C.; Ochterski, J. W.; Martin, R. L.; Morokuma, K.; Zakrzewski, V. G.; Voth, G. A.; Salvador, P.; Dannenberg, J. J.; Dapprich, S.; Daniels, A. D.; Farkas, O.; Foresman, J. B.; Ortiz, J. V.; Cioslowski, J.; Fox, D. J. *Gaussian 09 (Revision C.01)*; Gaussian, Inc., Wallingford, CT, 2010.

(34) Becke, A. D. *J. Chem. Phys.* **1993**, *98*, 5648−5652.

(35) Lee, C.; Yang, W.; Parr, R. G. *Phys. Rev. B* **1988**, *37*, 785−789.

(36) (a) Dunning, T. H., Jr.; Hay, P. J. In *Modern Theoretical Chemistry*; Schaefer, H. F., III, Ed.; Plenum: New York, 1976. (b) Hay, P. J.; Wadt, W. R. *J. Chem. Phys.* **1985**, *82*, 270−283. (c) Hay, P. J.; Wadt, W. R. *J. Chem. Phys.* **1985**, *82*, 299−310.

(37) Cossi, M.; Scalmani, G.; Rega, N.; Barone, V. *J. Chem. Phys.* **2002**, *117*, 43−54.

(38) (a) Casida, M. E.; Jamorski, C.; Casida, K. C.; Salahub, D. R. *J. Chem. Phys.* **1998**, *108*, 4439−4449. (b) Stratmann, R. E.; Scuseria, G. E.; Frisch, M. J. *J. Chem. Phys.* **1998**, *109*, 8218−8224. (c) Bauernschmitt, R.; Ahlrichs, R. *Chem. Phys. Lett.* **1996**, *256*, 454−464.

(39) *SPECFIT*; Spectrum Research Associates, Chapel Hill, NC.

(40) (a) Casado, A. L.; Espinet, P. *Organometallics* **1998**, *17*, 954−959. (b) Casado, A. L.; Casares, J. A.; Espinet, P. *Inorg. Chem.* **1998**, *37*, 4154−4156. (c) Robertus, J.; Reker, S. F.; Pijper, T. C.; Deuzeman, A.; Browne, W. R.; Feringa, B. L. *Phys. Chem. Chem. Phys.* **2012**, *14*, 4374−4382. (d) Glöckner, A.; Banneberg, T.; Ibrom, K.; Daniliuc, C. G.; Freytag, M.; Jones, P. G.; Walter, M. D.; Tamm, M. *Organometallics* **2012**, *31*, 4480−4494. (e) Howarth, A. J.; Davies, D. L.; Lelj, F.; Wolf, M. O.; Patrick, B. O. *Dalton Trans.* **2012**, *41*, 10150−10152.

(41) Helm, L.; Merbach, A. E. *Chem. Rev.* **2005**, *105*, 1923−1959.

(42) Kaim, W.; Reinhardt, R.; Sieger, M. *Inorg. Chem.* **1994**, *33*, 4453−4459.

(43) Feltham, R. D.; Metzger, H. G. *J. Organomet. Chem.* **1971**, *33*, 347−345.

(44) Altomare, A.; Cascarano, G.; Giacovazzo, C.; Guagliardi, A. J. *J. Appl. Crystallogr.* **1993**, *26*, 343−350.

(45) Sheldrick, G. M. *Acta Crystallogr., Sect. A* **2008**, *64*, 112−122.

(46) Farrugia, L. J. *J. Appl. Crystallogr.* **1997**, *30*, 565.

(47) Fenn, T. D.; Ringe, D.; Petsko, G. A. *J. Appl. Crystallogr.* **2003**, *36*, 944−947.